Marine and Petroleum Geology 116 (2020) 104310

Contents lists available at ScienceDirect

Marine and Petroleum Geology

journal homepage: www.elsevier.com/locate/marpetgeo

Research paper

Seismic stratigraphic patterns and characterization of deepwater reservoirs of the Mundaú sub-basin, Brazilian Equatorial Margin

Karen M. Leopoldino Oliveira[a,b,c,*], Heather Bedle[c], R. Mariano G. Castelo Branco[a,b], Ana Clara B. de Souza[a], Francisco Nepomuceno Filho[d], Márcio N. Normando[a], Narelle M. de Almeida[e], Thiago H. da Silva Barbosa[f]

[a] Programa de Pós-Graduação em Geologia, Universidade Federal do Ceará (UFC), Campus do Pici, Bloco 912, Fortaleza, Ceará, CEP, 60440-554, Brazil
[b] Laboratório de Geofísica de Prospecção e Sensoriamento Remoto (LGPSR). Universidade Federal do Ceará (UFC), Campus do Pici, Bloco 1011, Fortaleza, Ceará, CEP, 60440-760, Brazil
[c] School of Geosciences, University of Oklahoma, 100 East Boyd St. Suite 710 Norman, OK 73019, US
[d] Departamento de Física, Universidade Federal do Ceará (UFC), Campus do Pici, Bloco 922, Fortaleza, Ceará, CEP, 60440-554, Brazil
[e] Departamento de Geologia, Universidade Federal do Ceará (UFC), Campus do Pici, Bloco 912, Fortaleza, Ceará, CEP, 60440-554, Brazil
[f] Departamento de Engenharia do Petróleo, Universidade Federal do Ceará (UFC), Campus do Pici, Bloco 709, Fortaleza, Ceará, CEP, 60440-554, Brazil

ARTICLE INFO

Keywords:
Brazilian Equatorial Margin
Ceará Basin
Petroleum exploration
Deepwater environments
Turbidites
Magmatism

ABSTRACT

In recent years, the Brazilian Equatorial Margin has drawn attention due to its similarity to areas with new hydrocarbon discoveries in the African conjugated margin, and in French Guiana. However, studies on the tectonic regimes associated with transform margins and their evolution, structures, and petroleum potential are still lacking due to the geological complexity of this region. To address this knowledge gap, research has been done to better understand the geological structures, as well as to identify potential hydrocarbon accumulations in the deepwater Ceará Basin. To achieve this, we performed an integrated interpretation of a large 2D seismic data, new exploratory borehole data, as well as older well data with revised biostratigraphy. This data analysis refines the basin architecture and the Cretaceous-Paleocene tectonic evolution, including implications for hydrocarbon prospectivity in the Ceará Basin deepwater. 2D seismic interpretation was performed using modern concepts of continental break-up. To accomplish this, the transition of continental-oceanic crust was taken into account for restoration of the sediments of the rift stage in the basin. The analysis also identifies potential hydrocarbon accumulations in turbiditic reservoirs and presents new insights about the dimensions of the underlying rift features situated in the continental slope. The results reveal a high potential for drift sequences in deepwater where the Late Albian-Early Cenomanian-Turonian sediments reach thicknesses of approximately 3048–4894 m. Moreover, this research shows evidence of Cretaceous to Paleocene magmatism, indicated by the well-imaged volcanoes and associated sills in the seismic data. This analysis indicates that the Mundaú sub-basin can be classified as a volcanic passive margin that was developed during the oblique dextral separation between South America and Africa. The variety of stratigraphic and structural features developed through the Cretaceous history of the Mundaú sub-basin offers a variety of potential hydrocarbon traps and plays in a number of rift and post-rift sequences.

1. Introduction

The Brazilian Equatorial Margin (BEM) in northeastern South America and the eastern part of the Equatorial South Atlantic Ocean is composed by five sedimentary basins along the coast. There are, from west to east, the Foz do Amazonas, Pará-Maranhão, Barreirinhas, Ceará, and Potiguar basins (Fig. 1a). These basins began their development during the Early Cretaceous, as a series of several continental rift basins through a complex evolution with tectonic regime varying from predominantly normal (distension) to predominantly strike-slip

* Corresponding author. Programa de Pós-Graduação em Geologia, Universidade Federal do Ceará (UFC), Campus do Pici, Bloco 912, Fortaleza, Ceará, CEP, 60440-554, Brazil.
E-mail addresses: karenleopoldino@ou.edu (K.M. Leopoldino Oliveira), hbedle@ou.edu (H. Bedle), mariano@ufc.br (R.M.G. Castelo Branco), anaclarageologia@alu.ufc.br (A.C.B. de Souza), nepomuceno@fisica.ufc.br (F. Nepomuceno Filho), mnormando@gmail.com (M.N. Normando), narelle@ufc.br (N.M. de Almeida), thiagohenrique@alu.ufc.br (T.H. da Silva Barbosa).

https://doi.org/10.1016/j.marpetgeo.2020.104310
Received 6 September 2019; Received in revised form 17 February 2020; Accepted 19 February 2020
Available online 22 February 2020
0264-8172/

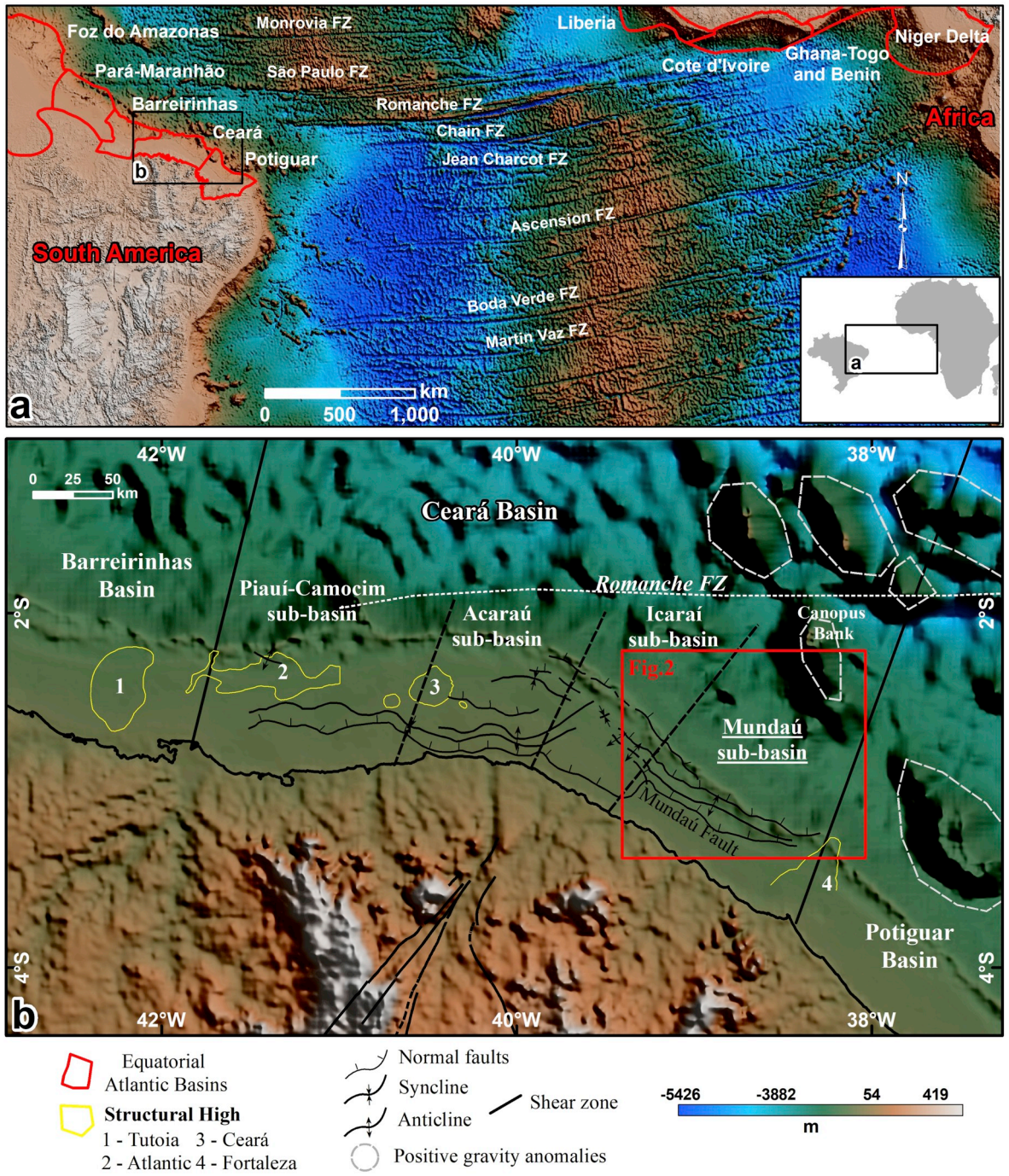

Fig. 1. (a) Regional topographic and bathymetric map of the Equatorial Atlantic showing conjugate margins in Brazil and Africa as well as the larger oceanic fractures zones in the area; (b) The Ceará basin is divided in four sub-basins: Piauí-Camocim, Acaraú, Icaraí and Mundaú. The Romanche Fracture Zone and positive gravity anomalies were mapped using data from the World Gravity Map (WGM2012). The topographic model is from the National Oceanic and Atmospheric Administration (NOAA). The structural data was compiled from Zálan and Warne (1985), Silva et al. (1999), and Morais Neto et al. (2003). The basin boundaries are from ANP and the sub-basins boundaries were adapted from Morais Neto et al. (2003).

(transtension and transpression) regime. The geological evolution of this margin is similar to the West African margin as Ghana, Ivory Coast and Liberia (Fig. 1a), being characterized a transform margin (Françolin and Szatmari, 1987; Matos, 1999, 2000; Milani and Thomaz Filho, 2000; Maia de Almeida et al., 2019).

In recent years, new hydrocarbon discoveries in the African conjugated margin, Brazilian margin and in French Guiana have drawn attention to the BEM. However, studies on the tectonic regimes associated with transform margins and their evolution, structures, and petroleum potential are scarce, partially due to the geological complexity (Zalán et al., 1985; Zálan and Warne, 1985; Soares et al., 2012; Nemčok et al., 2012; Krueger, 2012; Krueger et al., 2014; Davison et al., 2016; Maia de Almeida et al., 2019). Such basins and their structures require an in-depth research on their genesis and geological significance, especially for oil industry applications.

The exploration potential of Equatorial margins is exemplified by the Jubilee field in Ghana, which currently produces approximately 10,000 bopd only five years after the discovery (Karagiannopoulos, [updated 2018]). Other fields, also in Ghana's deepwater, such as Tweneboa-Enyenra-Ntomme (TEN) are also already producing oil. On

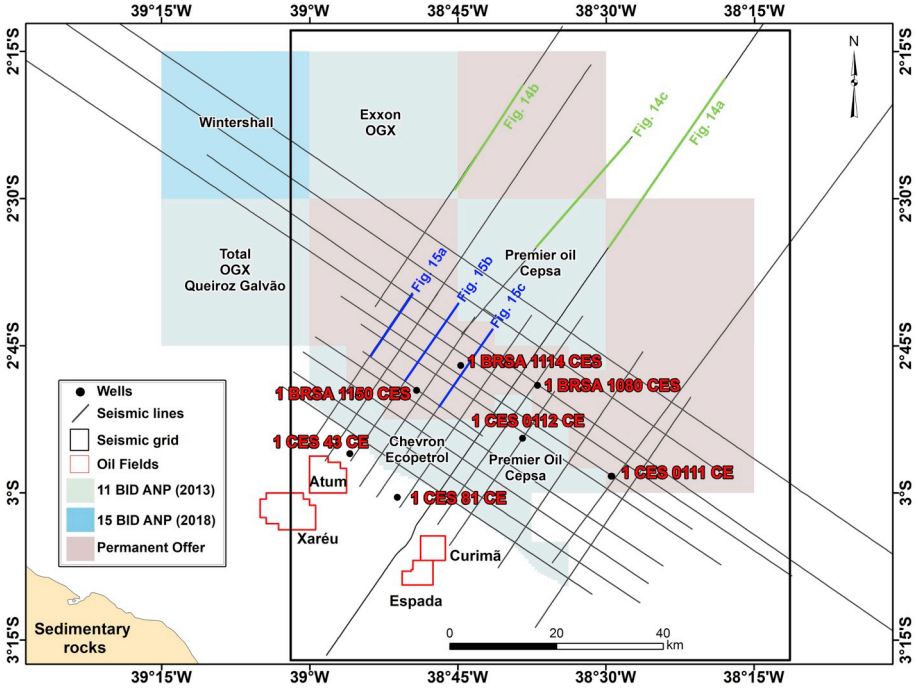

Fig. 2. The location of the wells, seismic data (2D), and the blocks of ANP Bidding Rounds are displayed. Also, four producer fields (Xaréu, Atum, Curimã, and Espada) in the Mundaú sub-basin are outlined. The black polygon frame indicates the area presented in Figs. 8–11.

the other hand, a much-publicized discovery in French Guiana was also announced in 2012 (Zaeydius field), however, six evaluation wells have since been classified as dry or with uneconomic (Zalán, 2015). Nevertheless, these analogue discoveries suggest potential for another world-class Jubilee-like oil system in deep and ultra-deepwaters of the BEM.

The 11th Round of Bids of the Brazilian National Agency of Oil, Natural Gas and Biofuels (ANP) in 2013 allowed dozens of blocks to be acquired by companies in all five basins of the BEM (Zalán, 2015). The ANP's most recent bidding round, the 15th in 2018, had 12 blocks offered in deep and ultra-deepwater in the Ceará Basin, totaling an area of approximately 8,500 km^2. According to ANP, BEM has potential for oil discovery in turbidite reservoirs from the late Cretaceous to the Paleogene, similar to the discoveries of the West African Margin. The increase in bidding in the last several years reveals the escalating interest in the hydrocarbon potential of the BEM.

The Ceará Basin is a frontier hydrocarbon producing basin with four fields in the shallow water domains of the Mundaú sub-basin (Xaréu, Atum, Espada and Curimã) (Figs. 1b and 2). In 2012, Petrobras drilled the 1 BRSA 1080 CES well, the first deepwater oil discovery in Ceará Basin, then two additional exploratory wells were drilled with more complete chronostratigraphic data collection. Two wells had previously been drilled in the deepwater in the 1990s, but data from these have not been publicly released, and thus are not correlated with the new wells.

Maia de Almeida et al. (2019) presented the petroleum system of the Mundaú sub-basin deepwater transitional sequence using the 1 BRSA 1080 CES well and seismic data. However, they did not discuss the potential reservoirs in the syn-rift and drift sequence. In this study, we improve the current geologic understanding of the basin, mapping the main geologic features using a large 2D seismic dataset, as well as identify regions of potential hydrocarbon accumulations in the deepwater Cretaceous-Paleocene sequences of Mundaú sub-basin. In addition, the seismic-stratigraphic interpretations are combined with new borehole data that includes detailed biostratigraphy data. This analysis results in a new understanding of the basin that can be used to identify possible plays and to refine the basin architecture and its tectonic evolution, including implications for hydrocarbon prospectivity in the Ceará Basin deepwater.

2. Geological setting

2.1. Ceará Basin

The Ceará Basin origin is related to the process of the Gondwana breakup during the Lower Cretaceous resulting in the Equatorial Atlantic opening. This basin is bounded to the east by the Fortaleza High, to the west by the Tutóia High, to the south by the Precambrian basement, and to the north by the Romanche Fracture Zone (RFZ) (Fig. 1b) (Costa et al., 1990). Due to the distinct tectono-stratigraphic character along and across the Margin, the Ceará Basin is divided into four sub-basins, from west to east: Piauí-Camocim, Acaraú, Icaraí and Mundaú (Morais Neto et al., 2003). The Piauí-Camocim is separated from the Acaraú sub-basin by the Ceará High. The Acaraú and Icaraí sub-basins have as common limit the Sobral-Pedro II lineament extension. In addition, the Icaraí is separated from Mundaú sub-basin by an important fault inflexion (Morais Neto et al., 2003).

Another defining characteristic of the basin are the intrusions and magmatic extrusions, which sometimes generate guyots and bathymetric highs. Only a few volcanic rocks are dated from the shallow water (continental crust) offshore the Ceará and Potiguar basins, and they reveal ages spanning from 83 to 28 Ma (Santonian to Lower Oligocene; Mizusaki et al., 2002; McHone, 2006). However, there is no direct sampling and dating of any offshore seamount from the BEM, except for the Fernando de Noronha Archipelago (Jovane et al., 2016). Therefore, there is no clear assessment of the relationship between sedimentation and volcanic rocks in the seamounts, and the current age estimate for the latest volcanic emplacement ranges between the Coniacian and the Eocene, and thus has an uncertainty of more than 40 My (Jovane et al., 2016).

2.2. Mundaú sub-basin

The Mundaú sub-basin is regionally structured by a major fault, the Mundaú Fault, which has normal offset in the NW-SE direction and is NE-dipping (Antunes et al., 2008) (Fig. 1b). The tectono-sedimentary evolution of the Mundaú sub-basin consists of three major

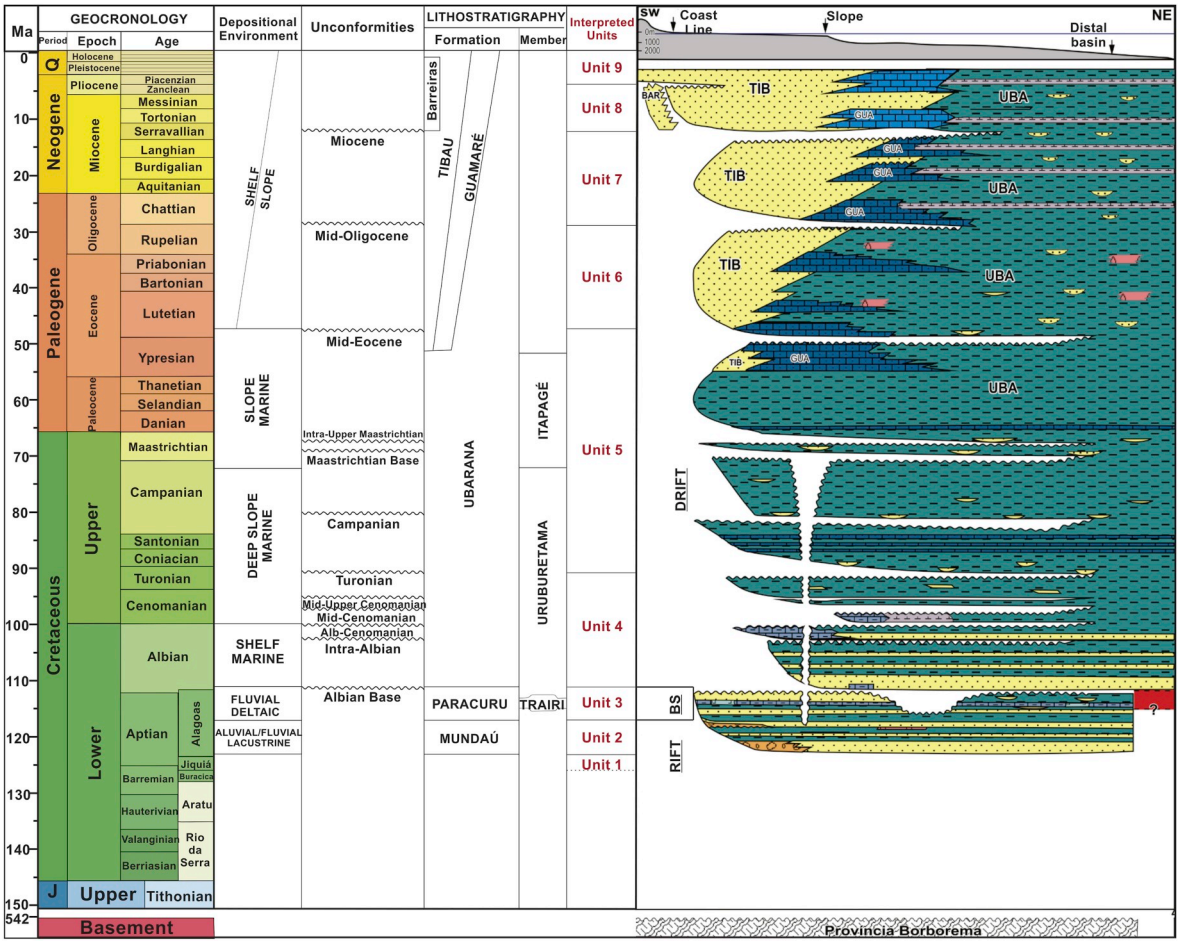

Fig. 3. Ceará Basin litho-, chrono-, and tectonostratigraphic columns with the representation of the units recognized in the study area (modified from Condé et al., 2007). BS: Breakup sequence; UBA: Ubarana Fm.; GUA: Guamaré Fm.; TIB: Tibau Fm.

megasequences (Beltrami et al., 1994): syn-rift, transitional, and drift. The syn-rift phase is characterized by the development of NW-SE normal faults forming asymmetric half-grabens, and continental sedimentation marked by fluvial-deltaic sandstones and shales of the Mundaú Formation (Beltrami et al., 1994). The top of this unit is a regional stratigraphic reflector, called the "Electric Mark 100" (Costa et al., 1990) or "1000" (Beltrami et al., 1994; Condé et al., 2007) and is interpreted to be the result of a period of regional flooding that affected the basin during the lower Aptian (Pessoa Neto, 2004).

The transitional sequence, the Paracuru Formation (Fig. 3), is marked by the first marine incursions recorded in the sub-basin, within the fluvial, deltaic, and lacustrine sandstones. Limestones and subordinate evaporites (Trairi Member) were also deposited at this stage (~115 My) (Costa et al., 1990; Beltrami et al., 1994; Condé et al., 2007).

The drift or marine megasequence developed as a result of continental drift and a marked phase of thermal subsidence. The Ubarana Formation (from ~110 My to 65 My) comprises two members (Fig. 3) (Costa et al., 1990; Beltrami et al., 1994; Condé et al., 2007). The first one, the Uruburetama Member (~110 My–75 My), corresponds to a marine transgression and consists of predominantly shales. The second member, Itapagé Member (from ~75 My to 65 My), corresponds to a regressive marine phase and consists of turbiditic shales and sandstones (Costa et al., 1990; Beltrami et al., 1994; Condé et al., 2007). The Guamaré Formation (from ~65 My to recent) consists of shelf carbonates, while the Tibau Formation (from ~65 My to recent) comprises proximal sandstones (Fig. 3). The clastic continental sediments of the Barreiras Formation comprise the youngest unit of the basin (Condé et al., 2007).

Magmatism in this basin occurred between the Mid-Eocene and Lower Oligocene. It was associated with a mafic event resulting in intrusive bodies of basalt and diabase, some of which were sampled in exploratory wells (Condé et al., 2007). Data from K–Ar and Rb–Sr dating (Mizusaki et al., 2002) indicate that the volcanic rocks vary in age from the Eocene (44 Ma, in the Ceará High area) to the Oligocene (32 Ma, in the Fortaleza High area). At north of Mundaú sub-basin there is a seamount named the Canopus Bank, which is a north-northwest–trending intrusion, 80-km long, 40-km wide, covering an area approximately 2,500 km^2. Its top reaches a depth of 150 m below sea level and is approximately 120 km^2 in area. Although seismic interpretation estimates the volcanic emplacement between 23 and 65 Ma, the hypothesis of seamount building because of multiple magmatic events is not disregarded (Maia de Almeida et al., 2019). Locally, near the Xaréu field (Fig. 2), a diabase sample provided a K–Ar age around 83 Ma, which may be related to the Cuó Magmatism - recorded in the Potiguar Basin and active in the Santonian-Turonian (Condé et al., 2007). Indeed, the geographical location and genetic determination of these rocks is essential for the geological study of the Ceará Basin, especially when it considers the influence of volcanic events in the generation, migration, and accumulation of hydrocarbons.

3. Data

This study is based on a large seismic reflection dataset and well data (Fig. 4), all of which were acquired by Petrobras and supplied by the Brazilian National Agency of Oil, Gas and Biofuels (ANP). We

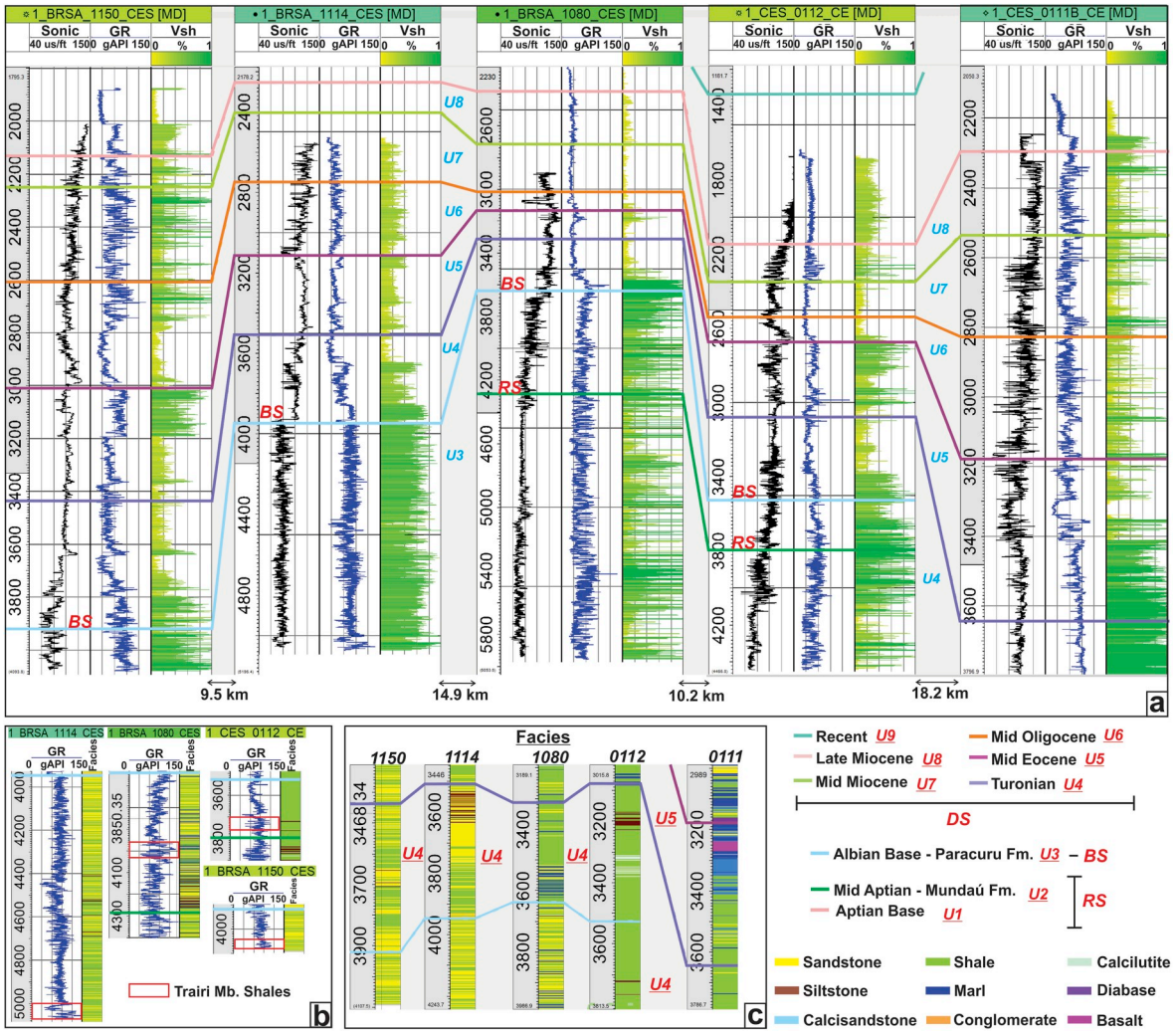

Fig. 4. (a) Correlation panel among the five deepwater wells showing interpreted seismic units, gamma ray, sonic logs, and calculated Vshale; (b) Four deepwater wells displaying the Paracuru Fm. interval of gamma ray and facies. The rocks of the Trairi Member are interbedded calcilutites and shales with high values of gamma ray. The 1 BRSA 1114 CES well data reveals that the Paracuru Formation in deepwater is composed of interbedded sandstones and shales in a subtle thickening pattern to the top; c) The five deepwater wells revealing the Unit 4 and 5 lithotypes. GR: Gamma Ray; Vsh: V shale; RS: Rift Sequence; BS: Breakup Sequence; DS: Drift Sequences.

interpreted more than 1,589 km of post-stack time-migrated multichannel 2D seismic reflection profiles located between the slope and the abyssal plain of the Mundaú sub-basin (Fig. 2). Additionally, two pre-stack seismic lines were processed to assist in the interpretation and for depth information. Seismic penetration to more than 9s TWT permitted the analysis of the entire seismic stratigraphic record of the abyssal plain down to the oceanic crust (Fig. 5). This data set covers an area of approximately 7,125 km^2, on a seismic grid of ~4 km spacing, which is sufficient enough to confidently tie the different seismic units mapped in this study.

The seismic sequence stratigraphic units were identified based on the newly available exploratory wells data 1 BRSA 1114 CES (2012), 1 BRSA 1150 CES (2013), 1 BRSA 1080 CES (2012), and older wells, including 1 CES 112 CE (1993), 1 CES 111 CE (1996), 1 CES 43 CE (1981) and 1 CES 81 CE (1983) which had revised biostratigraphy. These last two wells are located in shallow water. Well data includes standard log suites (i.e. gamma ray, density, resistivity, sonic, Vp, and Vs), checkshots, lithologic and geochemical data, formation tops, and biostratigraphic ages. Only three wells in deepwater have chronostratigraphic ages: 1 BRSA 1114 CES (2012), 1 CES 112 CE (1993), and 1 CES 111 CE (1996). This is the first deepwater study of the Ceará Basin where chronostratigraphic markers were used to refine the stratigraphic framework.

4. Methods

Seismic interpretations of horizons and faults were carried out in the time domain (TWT). These horizons correspond to boundaries of sedimentary formations recognized in the wells and to major lithologic discontinuities. These seismic profiles were analyzed following a conventional 2D interpretation methodology by mapping key high-amplitude reflectors, and then the generation of surface-time, surface-depth, and isopach maps. Geological interpretation of the seismic units was based upon the interpretation of seismic parameters, such as amplitude, frequency, continuity, and external and internal geometries, as well as on the classical concepts of sequence stratigraphy (Vail et al., 1977). Initially, chronostratigraphic information from 1 BRSA 1114 CES, 1 CES 112 CE, and 1 CES 111 CE was plotted on the seismic lines. The well correlation used primarily the gamma ray and the sonic logs data (Segesman, 1980) (Fig. 4). Then, the most significant reflectors were mapped, in terms of continuity, amplitude, and tied to the well data, which provided chronological meaning, and aided in defining the seismic sequences.

A frequency enhancing algorithm was employed to aid interpretation at both low and high frequencies. This algorithm is similar to Amplitude Volume Technique Attribute (AVT) introduced by Bulhões

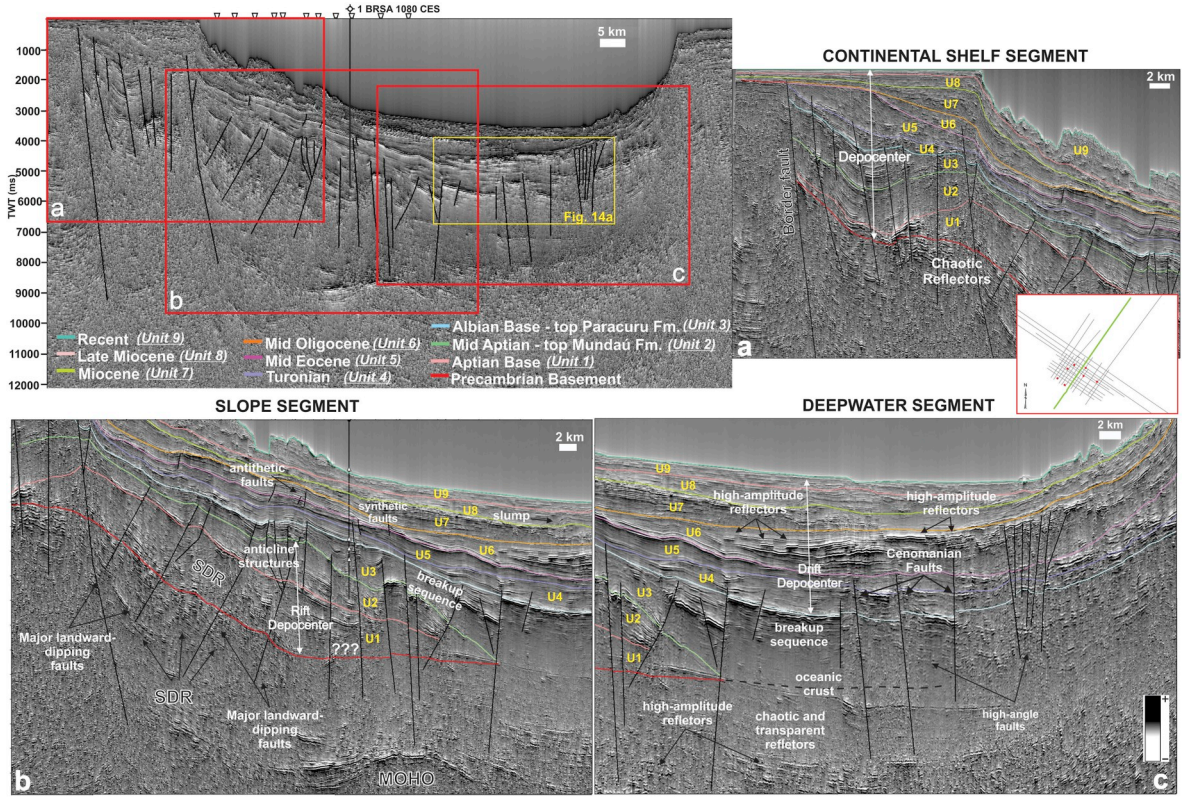

Fig. 5. Seismic section showing the continental shelf, slope and deepwater segments in the study area. (a) On the continental shelf, the border fault controls the extensional faults, which form half-grabens and the basin depocenter; (b) The slope segment is characterized by SDRs and the four major landward-dipping faults mapped in this basin. A thick rift depocenter as well as anticline structures are interpreted. Synthetic and antithetic faults are interpreted in drift sequence; (c) The deepwater segment is characterized by a thick drift sedimentary package, several high-amplitude reflectors, and high-angle and Cenomanian faults. The 1BRSA 1080 CES is shown in the up left. The Moho is interpreted on slope segment as a high-reflectivity zone around 9000 ms twt. Profile location (green line) is displayed on the right. Vertical scale in two-way traveltime (ms twt). The units mapped in this study are presented in yellow text. (For interpretation of the references to colour in this figure legend, the reader is referred to the Web version of this article.)

and Amorim (2005). By introducing frequencies that enrich the recorded reflections, an attribute is created that emphasizes seismic stratigraphic packages and assists their correlation throughout the seismic section. The packets, or sequences, thus defined, bring together sets of reflections that have similar acoustic impedance characteristics (Figs. 5–7).

We constructed a number of time-thickness (isochron) maps (Figs. 8 and 9) in order to highlight the regional configuration of the main depocenters, their spatial and temporal migration, and their relationship with the deep crustal architecture of the basin. The isopach map is a key resource in understanding the stratigraphic thickness of the sediments, and it also represents thickness variations within each depositional unit (Bishop, 1960). Isopach maps are essential tools in the erosional and depositional sedimentary reconstruction as well as the recognition of turbiditic bodies.

The major faults were picked and correlated from line to line. Next, the interval velocities of each seismic unit were obtained from checkshot data of the wells, so these interval velocities were finally corrected in order to fit the well tops. The defined velocity model was employed for a time to depth conversion. An average velocity obtained from the VSP of five deepwater wells was used. The average speed in the subsurface to the sedimentary package from Late Albian to Turonian interval was 2,668 m/s, while the average speed for water was 1,500 m/s. According to this data, it is inferred that the Late Albian-Early Cenomanian-Turonian depth is approximately 3048–4894 m in the deepwater and ultra-deepwater. Geochemical data from five deepwater wells were obtained from lateral rock samples, and 399 samples were analyzed for Total Organic Carbon (TOC) and Rock-Eval pyrolysis analyses. In all, this corresponds to 200 samples in the Late Albian to Turonian interval. These measurements were conducted in shales, sandstones, marls, and conglomerates belonging to Ubarana Formation.

5. Results

5.1. Seismic and structural interpretation

We here infer the tectono-sedimentary framework of the basin and its evolution based on seismic interpretation, structural, and isochrons maps. These maps were organized from oldest to youngest, focusing on the stratigraphic patterns and thickness trend. Nine major horizons were interpreted on the seismic lines (Figs. 5–8), which were chosen based on lithologic and chronologic data obtained from the composite well logs, and using the main unconformities present in this basin as first interpreted by Condé et al. (2007). From those horizons, nine isochrons maps were generated and named as units from one to nine. (Figs. 3 and 9). The tenth horizon, the seabed, was also mapped and is the top of the most recent sedimentary interval.

5.1.1. Basement

In the basement structural map (Fig. 8a), the transition from continental crust to oceanic crust corresponds to a change from basement depths of less than 4000 ms on the continental shelf to depths of more than 6000 ms on the toe of slope over more than 20 km. Differing from the Barreirinhas Basin, the transitional zone between oceanic and continental crust in this basin is wide (more than 20 km) (Figs. 5, 8a and 10), as a result of being located between oceanic fracture zones. The basement was better identified at deepwater basin region, as the seismic lines tend to lose resolution in deeper parts at continental shelf.

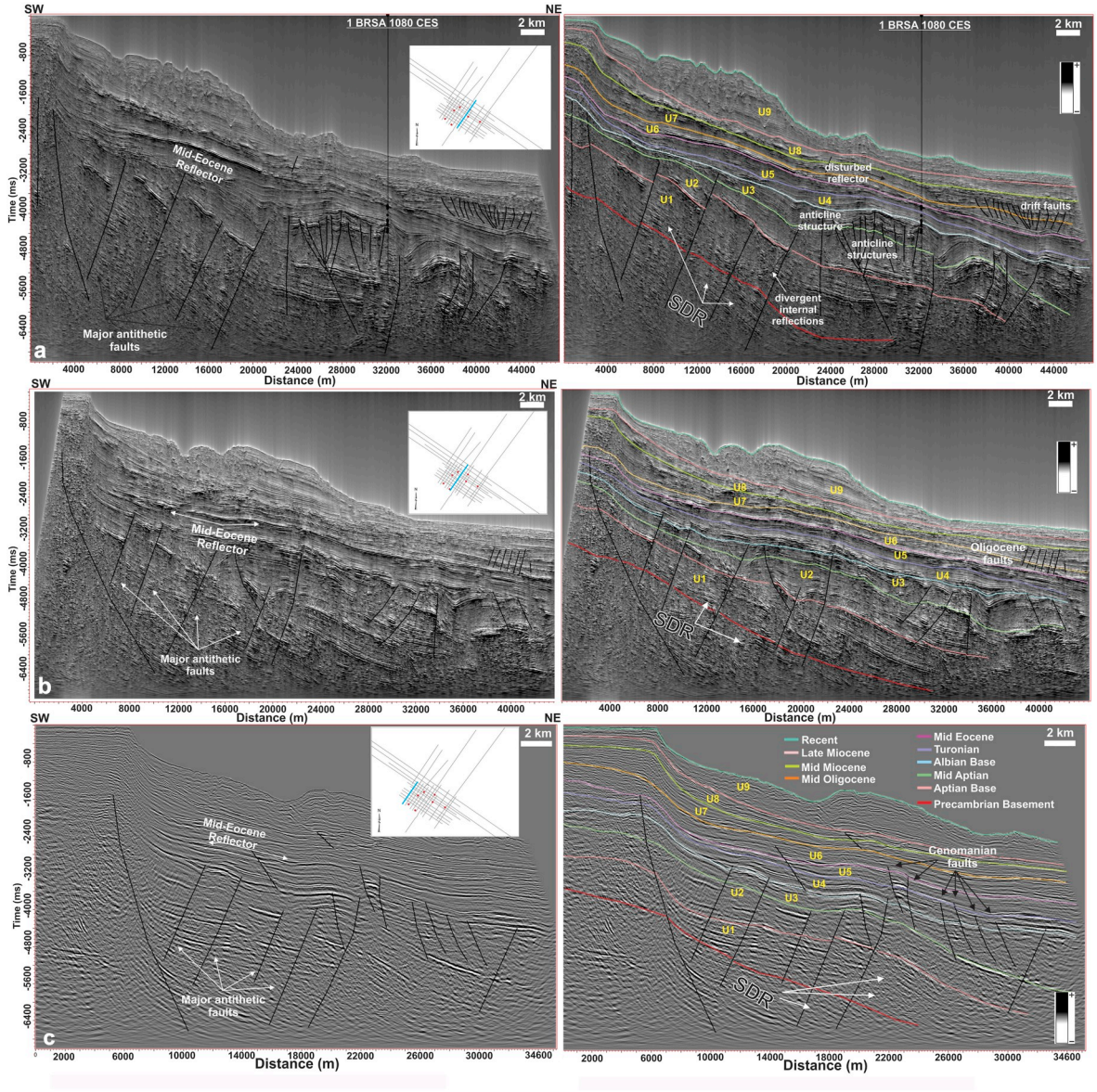

Fig. 6. SW-NE dip seismic sections with stratigraphy uninterpreted and interpreted. The uninterpreted sections show the major antithetic faults and Mid-Eocene reflector. a) Interpreted section shows several anticline structures on the continental slope where it is related to the rift stage. Oligocene faults are shown in this section. Reflector SDRs were interpreted in the basement. The 1 BRSA 1080 well and its hydrocarbon evidence are labeled (black dots); b) Oligocene faults and SRD reflectors were also interpreted in this section; c) Interpreted section shows the interpreted horizons and Cenomanian reactivation faults. Note that seismic in C AVT attribute was not applied. The location is depicted in all the stratigraphic uninterpreted sections. Vertical scale in two-way traveltime (ms twt). The units mapped in this study are presented in yellow text. (For interpretation of the references to colour in this figure legend, the reader is referred to the Web version of this article.)

The basement is seismically characterized by chaotic internal reflectors at the continental shelf and contains seaward dipping reflector (SDR) in the continental slope and deepwater. This region is commonly cut by normal faults composed by horsts and grabens (Fig. 5a). On the continental shelf, the basement of the Ceará Basin is composed of Borborema Province rocks (Morais Neto et al., 2003). The basement of the ultra-deepwaters is composed of basaltic rocks of oceanic crust. Oceanic crust is characterized by transparent or chaotic seismic facies. In these facies, the presence of diffraction is noted in the upper part, and high-amplitude are observed in the lower portion near the Moho (Fig. 5c). Fig. 8a displays a trend of the shallower basement to the southeast of the area, while the basement trends to the northwest at greater depths. The basement high in the south is related to the continental shelf. In the south, locally poor quality and less availability of seismic data increases uncertainty in the interpretation.

5.1.2. Unit 1 (Aptian base)

The Aptian base sequence U1 defined in this study underlays the basement and is below the Mid Aptian sequence that corresponds to the top of Mundaú Formation (Figs. 5–7 and 8b). In shallow waters, beneath the top of Mundaú Formation, there are well-marked discontinuities in electric profiles, informally denoted as the 700 and 800 marks, which are consecrated by use for by over 30 years of exploration in the basin (Condé et al., 2007). Analyzing the seismic lines in deep-water (Figs. 5–7), along with well data, there are some well-marked reflectors which allow a subdivision of the Mundaú Formation based on seismic facies. The top of this unit was defined as the Aptian base, based on previous research where the rocks have a high source rock potential (Falkenhein et al., 2001). There is no information about rocks older than Aptian, however, Condé et al. (2007) suggested that there may be older deposits in the deepest portions of the basin and they could be correlated to the Pendência Formation (Barremian age) of Potiguar

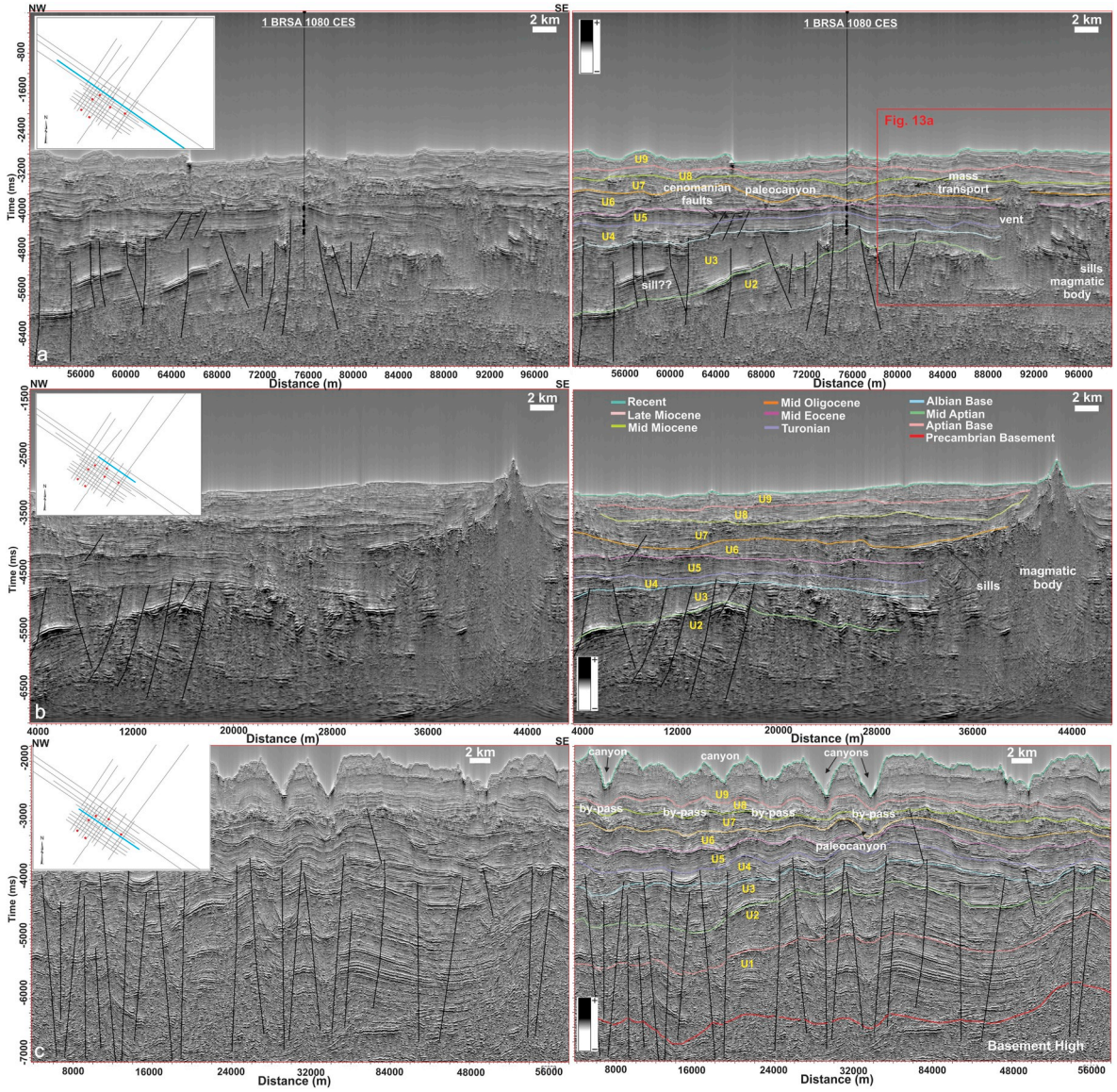

Fig. 7. NW-SE strike seismic sections with stratigraphy uninterpreted and interpreted and the location of the BRSA 1080 well is shown together with the location of hydrocarbon evidence (black dots); a) Interpreted section showing the presence of magmatic bodies as sills and vent. Mass transport and a paleocanyon is interpreted in the drift sequences. Red polygon indicates the area displayed in Fig. 13a; b) Several sills and a magmatic body are shown in this section; c) Paleocanyons, canyons, and a basement high were interpreted in this section. The location is depicted in all the stratigraphic uninterpreted sections. Vertical scale in two-way traveltime (ms twt). The units mapped in this study are presented in yellow text. (For interpretation of the references to colour in this figure legend, the reader is referred to the Web version of this article.)

Basin. The thicker package of this unit in seismic images (Figs. 5–7) corroborate that older rocks could be present.

This interval has seaward dipping reflectors in the slope with high-amplitude and continuous to sub-continuous, locally chaotic reflections with divergent patterns near faults (Fig. 6a), which are indicative of syn-tectonic deposition. In the deepwater, this formation has high-amplitude, concave downward reflectors, parallel, and continuous reflections (Figs. 5 and 6). It pinches-out approximately 40 km off of the continental shelf where the continental crust ends (Fig. 5), and its deposition had a thicker distribution to the east of the slope (Fig. 8b).

The faulted blocks often show parallel and high-amplitude reflectors to divergent and transparent reflector when approaching the faults indicating the presence of early syn-rift sediments infilling the grabens (Figs. 5 and 6). On the continental shelf, basinward-dipping faults form rotated blocks establishing a half-graben system. Convex, continuous to sub-continuous seismic reflections, sometimes presenting high-amplitudes, are observed inside the grabens. Normal faults affect the continental crust below the continental shelf. The continental slope displays this unit as filled horsts and grabens related to the complex evolution of this basin controlled by landward-dipping faults (Figs. 5–7, 8b and 9a). The greatest thickness (maximum of 1600 ms) of this sequence in relation to the basement is in the central region, following a trend NW-SE, while small values are on the continental shelf and in the north are due to contact with the continental crust boundary (Fig. 9a). The isochron map of this unit shows that most of the sedimentary package, up to 1300 ms (Fig. 9a), was accumulated on the continental slope, filled grabens.

5.1.3. Unit 2 (Mid Aptian)

The Mid-Aptian unit corresponds to the Mundaú Formation, which has another well log correlation and a strong reflection in seismic lines. The top of this unit is represented by the Mid-Aptian structural map (Fig. 8c). Two wells in deepwater reach the top of this unit. Similar to the previous unit described above, this interval also has seaward

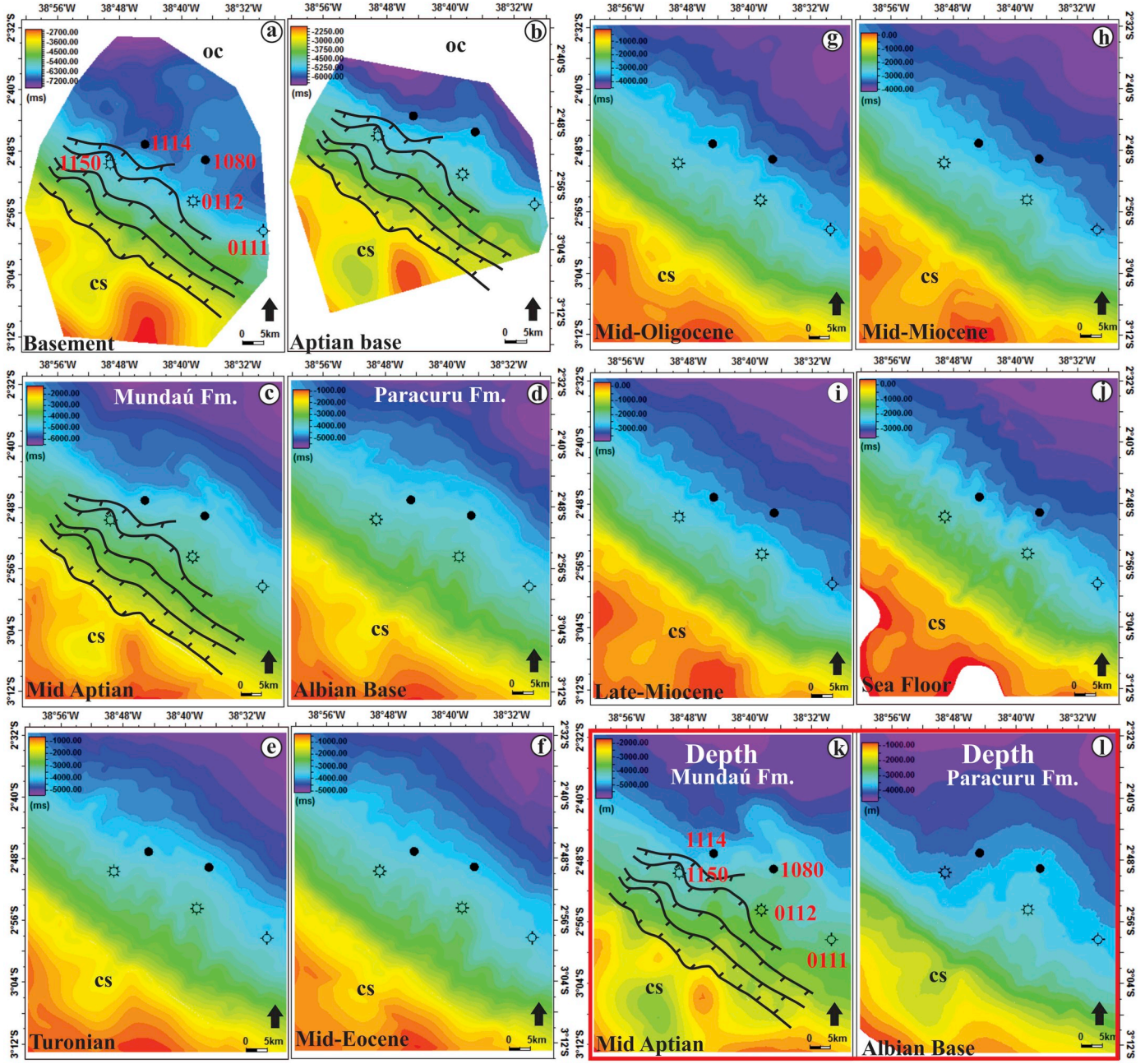

Fig. 8. Structural maps from ten major horizons interpreted with seismic, and two structural maps migrated in time and depth. The location of five deepwater wells and the four major faults are shown. Parts (a) through (j) display time structure maps, parts (k) and (l) display depth structures. CS: continental shelf; OC: oceanic crust.

dipping reflectors. However, its seismic facies patterns are not homogeneous. Its upper part is predominantly marked by chaotic reflections, while strong and continuous reflections are marked in its lower part (Figs. 5–7). The continental slope is composed of both highs and lows of this formation, having uniform sedimentary dispersion in the center and its greater depths lie at the north (Fig. 8c), where continental crust ends. This formation shows downlap over the early oceanic crust formed on the northern part of the basin (Fig. 5b). Fig. 8k shows the extent of this surface in depth.

The top of the rift stage, on the continental shelf and in deepwater, is represented by this unit. Rift-related basement faults formed horsts and grabens within the area of the current continental shelf (Fig. 5a and 9b). The syn-rift sequence (Unit 2) is very thick in the study area, with more than 1000 ms of sediments. The depocenter within the extent of the modern continental shelf reflects the adjustment between the border fault and the fault near the slope (Fig. 5a). When compared with the previously described sequence, Unit 1, the syn-rift sequence has the greatest thickness (maximum of 1250 ms) in northeast of the area, while a slight thinning of this sequence is observed on the southeastern side of continental slope (Fig. 9b).

5.1.4. Unit 3 (Albian Base)

The base of this sequence is the Mid Aptian horizon (Fig. 8c) and the top of the sequence is the Albian Base horizon (Fig. 8d) that corresponds to the top of Paracuru Formation. This unit is considered a breakup sequence (Soares et al., 2012) as its deposition comprises an unconformity-bonded stratigraphic interval, which was controlled by the tectono-stratigraphic events triggered by the breakup. At this age, the oceanic crust began to form and this sequence is overlying it, being the first sequence to be deposited on top of oceanic crust (Figs. 5 and

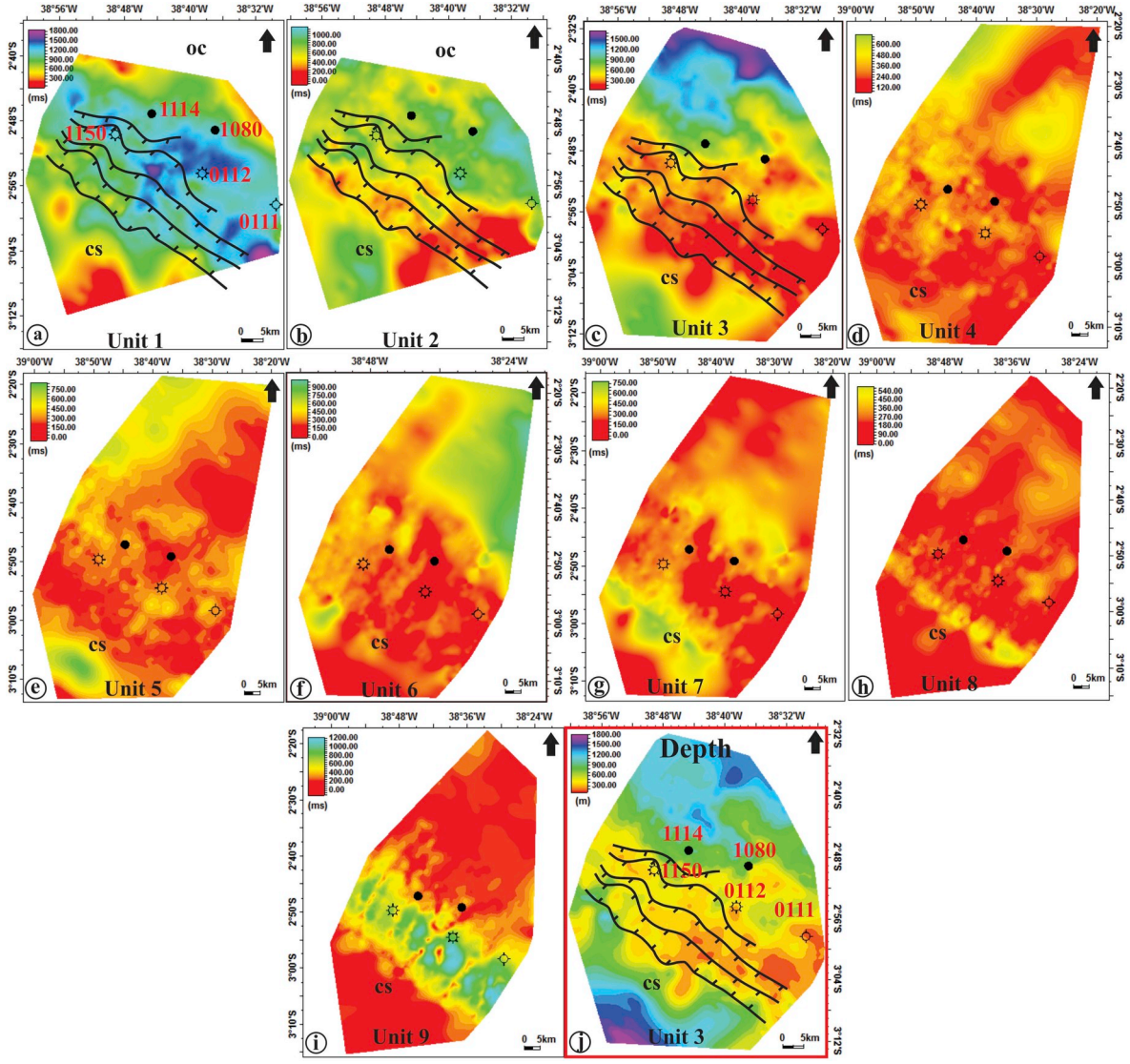

Fig. 9. Isochron maps from eight units from the studied seismic lines, and one isochron map migrated in depth. These maps show sediment thickness distribution. The location of five deepwater wells and the four major faults are also shown in the figure for reference. Parts (a) through (i) display time structure maps, part (j) displays the depth structure. CS: continental shelf; OC: oceanic crust.

10). The breakup was finalized during the lower Albian in this segment of Equatorial Margin, where syn-wrench sedimentation took place (Falkenhein et al., 2001). This unit has seismic facies that are parallel to sub-parallel, high amplitude and continuous reflectors. The sequence becomes thicker in the distal part of the basin, especially in the northwest. Unlike the previously described sequence that has a uniform sedimentation in the northeast of the area, this already has a more uniform distribution, even if subtle, to the northwest, making the area more regular in terms of deposition (Fig. 8d). The greatest thickness (maximum of 1600 ms) of this sequence in relation to Unit 2 is in the extreme north (Fig. 9c). The small values are on the continental slope mainly in southeast, highlighting one NW-SE trending, elongated feature in northeast (Fig. 9c). Fig. 8l shows the coverage of the top horizon of this unit in depth. Some magmatic features interpreted as sills were imaged by high-amplitude reflections (Fig. 7a and b).

The entire Aptian-Albian interval, as well as underlying sequences, are cut by normal faults, suggesting active tectonic in these ages. The 1 BRSA 1080 CES well, where oil was discovered, was positioned where there is a high of Mundaú Formation formed by a fault and probably mobile shales (Fig. 6a). The isochron map between the top of Mundaú Formation and the top of Paracuru Formation (Unit 3) reveals that the sedimentary depositional preference to the northwest has greater thicknesses, while the continental slope has smaller thickness values, mainly in the east (Fig. 9c). Fig. 9j displays the depth thickness of unit.

5.1.5. Unit 4 (Albian Base-Turonian)

This Unit marks the beginning of the drift sequence. Its base is composed of conglomerates representing deposits of low sea system tract (Figs. 4c–1 BRSA 1150 CES and 1 BRSA 1114 CES wells), and seismically is composed of plane-parallel and high-amplitude seismic reflectors (Figs. 5 and 6). The top of this unit corresponds to a Turonian age horizon (~89 Ma) (Figs. 5 and 10) related to a maximum flooding surface and anoxic event that has a very characteristic high-amplitude seismic character, and can be easily correlated throughout the Equatorial margin (Trosdtorf et al., 2007). The 1 BRSA 1080 CES and 1 CES 0112 CE wells present a low sand supply during the deposition at the base of this sequence, while the shale input was high, representing predominantly shelf to deepwater environments (Fig. 4c). However, the 1 BRSA 1114 CES and 1 BRSA 1150 CES reveals a high sand supply in the whole sequence (Fig. 4c). The structural map presents increased depths in the northwest of study area, with regular sediment distribution on the continental slope (Fig. 8e).

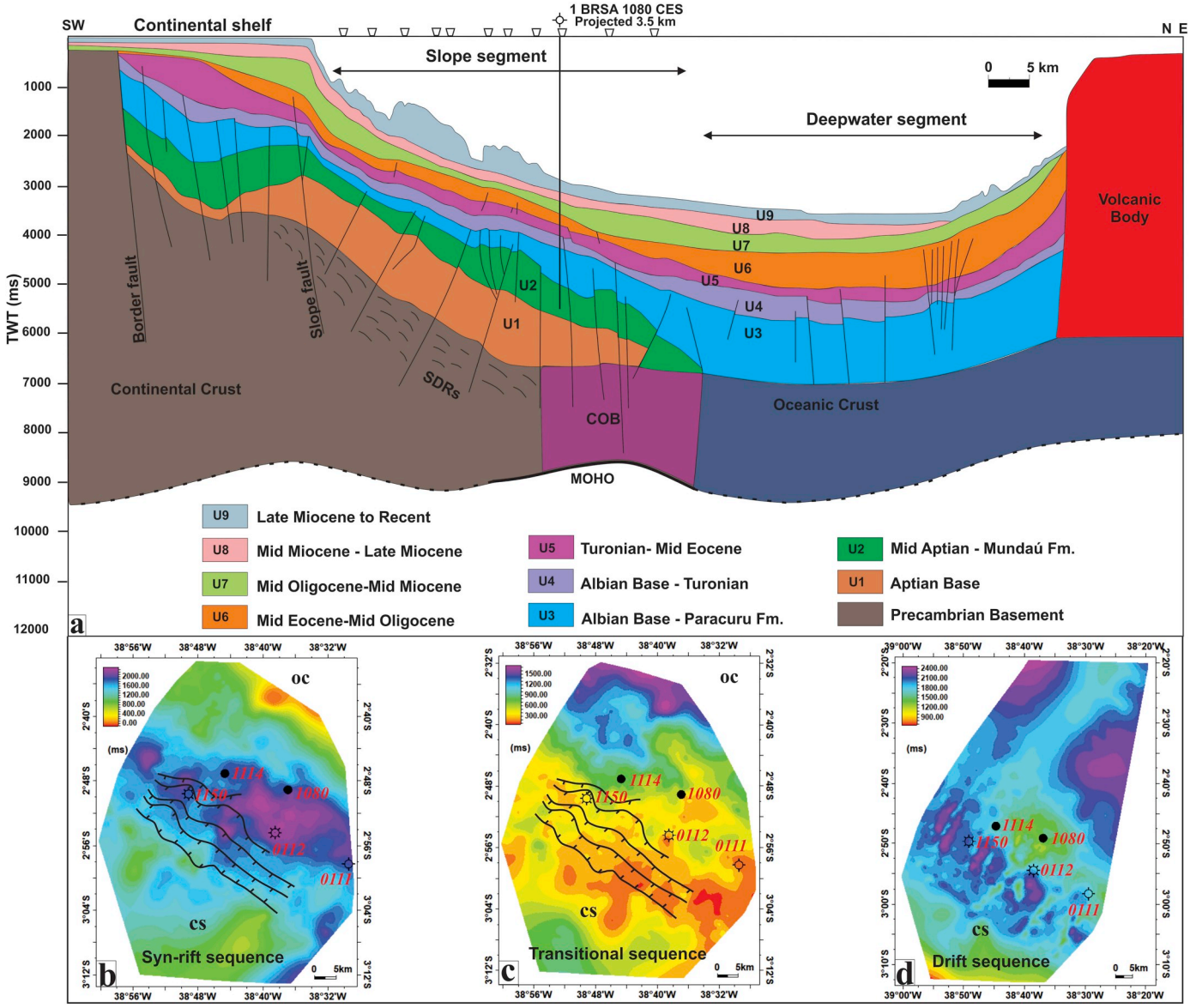

Fig. 10. (A) SW-NE schematic geological section showing the architecture of the segments and stratigraphic interpretation. Note the thick package of rift sequences in the continental slope segment, and the thick package of drift in the deepwater segment. The projected location of the BRSA 1080 well, the oil discovery, is marked. (B) The isochron map of the syn-rift sequences. (C) The thickness map of the Transitional sequence (breakup sequence). (C) The thickness map of the drift sequences. COB: Continental-oceanic boundary; CS: continental shelf; OC: oceanic crust; TWT: two-way traveltime.

The Cenomanian faults have a similar orientation to the rift faults, which seem to be linked at depth (Fig. 5b and c). This suggests that the Cenomanian faults formed as a result of a phase of reactivation of the older and deeper rift structures. Given the evidence that rifting terminated in the late Aptian (Figs. 5 and 10), the extensional phase responsible for the formation of these late faults may have been triggered by processes of 'post-rift relaxation' (Morgan, 1983; Burov and Cloetingh, 1997; Burov and Poliakov, 2003). The lack of known regional tectonic events in the margin during the Late Cretaceous makes it difficult to suggest alternative scenarios for the formation of the Cenomanian faults. The isopach map of this interval (Unit 4) shows smaller thickness when compared to the others due to the large number of erosive events that occurred in this period (four events in 10 Ma) (Condé et al., 2007) (Fig. 3). Beyond that, most of the sediments, up to 500 ms, were accumulated on the continental slope in a ponded depocenter (Figs. 9d and 11a). Thick sedimentary packages are observed in the deepwater suggesting that the sediments also bypassed this area and continued further downslope (Fig. 11a). The thickness, when compared to the previous unit above described, is smaller. It reaches a greater depth to the northeast and northwest, with a thin feature among them following a trend NE-SW, probably associated with the Romanche Fracture Zone structures.

5.1.6. Unit 5 (Turonian-mid Eocene)

The top of this is represented by Mid-Eocene unconformity horizon (Fig. 8f) that is very expressive in this basin, especially in distal areas. It is the seismic reflector most representative of drift phase, with a high acoustic impedance, in all of the deep and ultra-deepwater seismic lines (Fig. 6). In this sequence, during the Campanian (~78 Ma), the sea level dropped, marking the change from mainly transgressive to regressive sequences (Trosdtorf et al., 2007). The Maastrichtian was a time of tectonic quiescence, and in this basin sediments were deposited in a regressive sequence called the Itapagé member (Condé et al., 2007). This interval is composed of plane-parallel, sometimes continuous or chaotic seismic reflections (Figs. 5–7). This interval has greater thicknesses on the continental

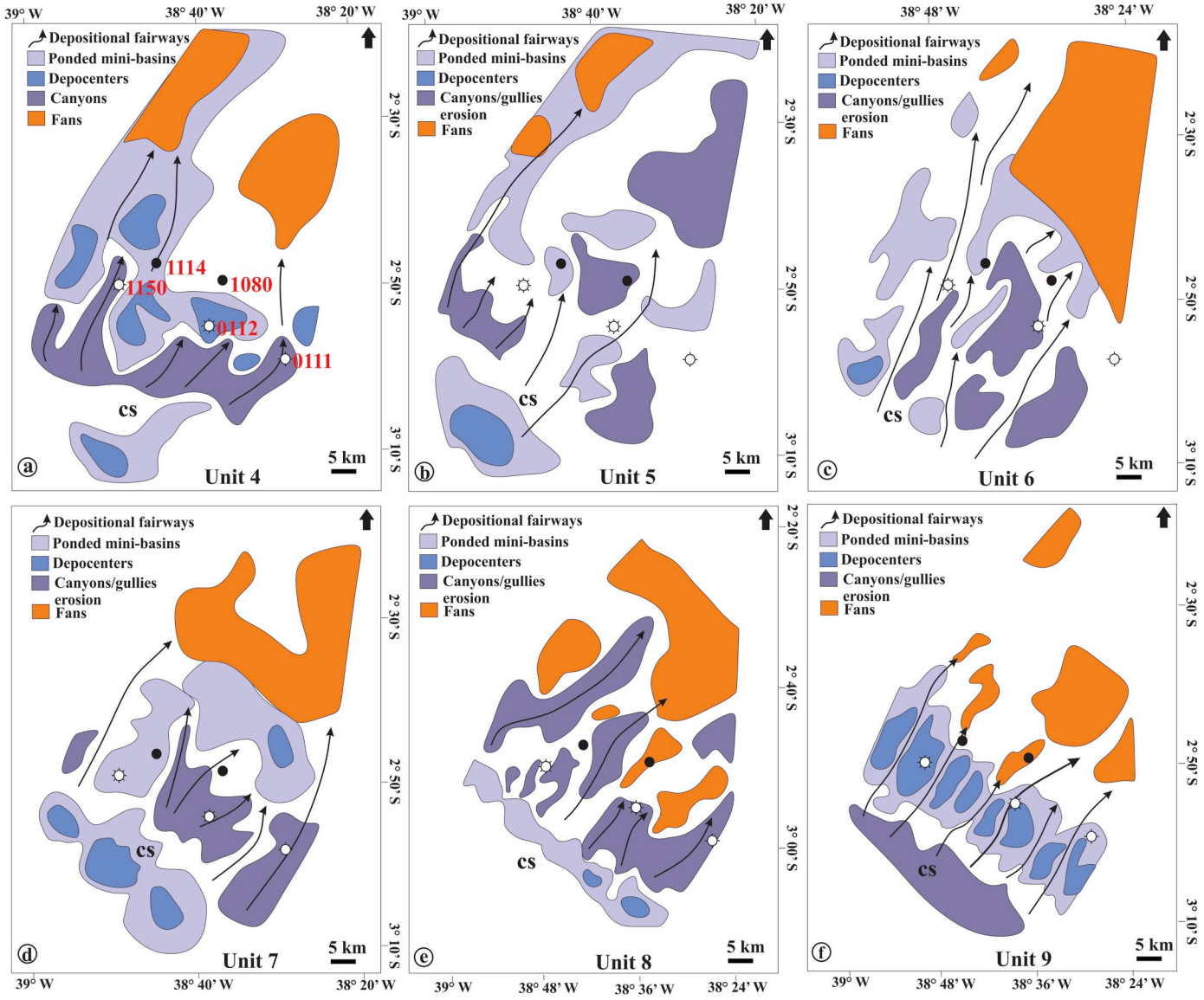

Fig. 11. Interpreted depositional environments in the drift units and location of the five deepwater wells used in this study. The drift deposition in slope segment reveals an active dynamic of erosion with canyons and gullies developed during its evolution. CS: continental shelf.

shelf and to the northwest of the distal part of the sub-basin (Fig. 9e). It has a more uniform sedimentary distribution in the western portion of the study area. The 1 BRSA 1150 CES and the 1 CES 111 CE wells have greater thickness of this unit, while the 1 BRSA 1080 CES well has smaller thickness (170 ms) (Figs. 4a and 9e).

On the continental slope, this sequence is intersected by basinward-dipping faults (Fig. 6c). In the deepwater, this sequence is intersected by vertical faults related to the reactivation of the Romanche Fracture Zone and emplacement of magmatic bodies (Fig. 5c). The isochron map between the Turonian and Mid-Eocene (Unit 5) shows the depositional thickening infilling a Turonian ponded depocenters, which are wider (up to 10 km in the continental shelf) than the Late Albian mini-basins, represented on the Late-Albian to Turonian isochron (Fig. 9d). Comparing these isochron maps, some Late Albian mini-basins coalesced into larger basins during Turonian time, while others were buried. As previously described above, depositional thickening is observed in the northwest region, suggesting sediments also bypassed the area into the deepwater (Fig. 11b). The continental shelf has a better sedimentary distribution due to adjustment of the border fault and to the regressive event related to the Itapagé Member (Figs. 5 and 11b).

5.1.7. Unit 6 (mid Eocene – Mid Oligocene)

The top of this unit is represented by a Mid Oligocene unconformity (Figs. 5–7 and 8g). The structural map reveals that this unit has greater depths in the north trending to NW-SE direction (Fig. 8g). Seismic facies are parallel to sub-parallel, often with a high-amplitude and continuous reflector. It has a strong seismic reflector and is well-marked on electrical profiles (Figs. 4 and 6). The top of this unit corresponds to the Rupelian-Chattian boundary unconformity (Trosdtorf et al., 2007). During the Oligocene, conditions changed from regressive in the Rupelian to transgressive in the Chattian, and formed the Oligocene unconformity (Haq et al., 1987). This interval is thicker on the northeast part of the distal sub-basin, and thinner in the continental shelf and the continental slope from the center to the east (Fig. 8g).

The isochron map (Fig. 9f) between the Mid-Eocene and the Mid Oligocene unconformity (~27 Ma) horizons represents the thickness of Unit 6. On the continental shelf and on the continental slope most of sediments were eroded and deposited into deepwater environments, mainly in northeast of this basin (Fig. 11c). On the continental shelf there are three Mid-Eocene mini-basins and additional sedimentary deposition occurring to the west of the continental slope (Fig. 9f). At the toe of the continental slope, this sequence is intersected by oceanward-

dipping faults that change their direction to landward-dipping faults (Fig. 6a).

5.1.8. Unit 7 (Mid Oligocene-Mid Miocene)

The top of this unit corresponds to a Mid-Miocene age horizon (Figs. 5–7, 8h, and 10) that is related to the top of a large transgressive event observed across the whole Brazilian Equatorial Margin, which gave origin to a large carbonate ramp (Trosdtorf et al., 2007). Seismic facies are uniform, parallel, and continuous reflectors. Common zones of internal disturbed reflections related to high sediments input have been recorded (Fig. 7a). In the continental slope there are transparent zones in seismic data associated with depositional changes and is characterized by the presence of disturbed discontinuous seismic reflection (Fig. 6a). The structural map presents a uniform sedimentary deposition in the study area, with depths ranging from 500 ms in the continental slope to 4300 ms in distal part (Fig. 8h). The greatest thickness (maximum of 700 ms) of this unit in relation to Unit 6 is in the upper and lower slope, which trends to the NW-EW, while the small values are on the middle slope and the northwestern distal region (Fig. 9g).

This was a time of erosion on the continental slope and deposition as its toe, as gullies and channels are observed on the slope (Fig. 11d). The isochron map for this sequence (Fig. 9g) shows that in the continental shelf three Mid-Eocene depocenters became wider, and the continental slope was partially eroded and sediments were deposited in its toe (Fig. 11d).

5.1.9. Unit 8 (mid Miocene to Late Miocene)

The structural map of Fig. 8i presents the top of this unit, Late Miocene age, as an irregular relief in the continental slope. The relatively continuous reflectors with different impedance contrast indicate the existence of lithological intercalation between sands and clays (Fig. 4a – Vshale). The greater thickness of this unit is in the upper continental slope, while the slope was eroded at this time forming bypass zones to sediments supplies in deepwater (Figs. 7c and 11e). Like Unit 7, the structural map presents a uniform sedimentary deposition with depths ranging from 400 ms in the continental shelf to 3500 in distal part (Fig. 8i).

The isochron map between these horizons (Unit 8) represents the sedimentary deposition during these ages (Fig. 9h). The top of the continental slope has the greatest thickness.

5.1.10. Unit 9 (Late Miocene to recent)

Currently, the sea floor is a highly eroded surface cut by canyons (Fig. 7c) with unconsolidated sediments. The greater depths of this unit are in the northeast (Fig. 8j). The greatest thickness (maximum of 1200 ms) of this unit in relation to Unit 8 is in the continental slope (Fig. 9i) revealing an increase in the sediment supply in the Ceará Basin. This deposition dynamic was also observed by Krueger (2012) in the Barreirinhas Basin, which had a deformation episode at this age that coincides to paleogeographic changes in the north of South America.

The Late Miocene to recent isochron map (Fig. 9i) represents the sedimentary accumulation in Unit 9. Sediments are thicker in the eastern region of the continental slope (Fig. 11f). The Late Miocene progradation that took place on the Brazilian Equatorial margin is not only related with the global cooling, but also to the adjustment of the drainage system due to an Andean tectonic event (Altamira-Areyan et al., 2009).

The toe of the continental slope has been eroded in the Upper Miocene age and continues to be eroded allowing sediments to be deposited in the abyssal plain, mainly in the NW and NE domains of this basin (Fig. 11f).

5.2. Well data

The sedimentary package of the rift stage reveals a significant thickness, sampled in the 1 BRSA 1080 CES well, of approximately 1600 m, which reached the greatest depth of the Mid Aptian Mundaú Formation (Fig. 4a). The base of the rift stage has not yet been reached by any of the deepwater wells in this basin to date.

Analyzing the data from the five wells drilled in the deepwater of the Ceará Basin, four of these reached the Late Aptian Paracuru Formation; however, only two sampled the entire depth of the interval: the 1 CES 112 CE and the 1 BRSA 1080 CES (Fig. 4a). In both, the total thickness was approximately 302 m and 647 m respectively, with the latter having 86 m more than the total thickness reported for this formation by Beltrami et al. (1994). Also, the 1 BRSA 1114 CES well crosses more than 1170 m of the Paracuru Formation without reaching its base (Fig. 4a). Out of these, more than 1000 m overlies the Trairi Member (81 m), which means that the upper interval of the Paracuru Formation in this well is thicker than 1000 m (Fig. 4b).

The stratigraphic chart of this basin shows 5 My as the duration of sedimentary deposition established for the Paracuru Formation (Condé et al., 2007) (Fig. 3). An estimation of sedimentation and depositional age can be made, as the entire formation has three different lithologic units which occurred in 5 My. This reveals that the 1000 m of the upper interval in the 1 BRSA 1114 CES well would have been deposited within approximately 1.7 My, with a sedimentation rate of 588 m/Myr. This value is high for the depositional patterns sag-like basins, as interpreted by the depositional environment of the Paracuru Formation (Beltrami et al., 1994; Morais Neto et al., 2003). This analysis corroborates the Condé et al. (2007) assumption that the sediments deposited in this formation were influenced by active tectonism. This also is shown in the seismic interpretation of this work, and in that of Maia de Almeida et al. (2019).

Well data reveals that the Paracuru Formation in deepwater is composed of interbedded sandstones and shales in a subtle thickening pattern to the top (Figs. 4b–1 BRSA 1114 CES well). Also, the 1 BRSA 1114 CES well reveal that there was a progressive infill of the basin no matter what the depositional environment of that formation was. The rocks of the Trairi Member as sampled by four wells are interbedded calcilutites and shales, and these shales present high values of gamma ray (Fig. 4b). Condé et al. (2007) described this formation in shallow waters as a rich organic matter shales, proving this range has hydrocarbon potential. Maia de Almeida et al. (2019) used geochemical data from 1 BRSA 1080 CES, and described the rocks of Paracuru Formation to have good generation potential based on the good to very good amount of organic matter present.

Siliciclastic reservoirs in the rift and transitional sequences, having similar shallow water fields as their analogue basins, were targeted in four wells. In one case (1 CES 0111 CE), the well did not reach the target section; in two cases (1 CES 0112 CE and 1 BRSA 1114 CES), the siliciclastic reservoirs of the Paracuru Formation were of low quality. In the most successful case (1 BRSA 1080 CES), oil was found in sandstones of this same formation, well test results were promising and reliable but the quantity is not yet commercially viable (Maia de Almeida et al., 2019).

On the other hand, the oil found in Ubarana Formation is 40°API and gas oil ratio 136 m^3/m^3 as sampled in the 1 BRSA 1114 CES well. In the only case of hydrocarbon presence, the 1 BRSA 1050 CES well, which targeted deepwater turbidites of the Ubarana Formation, no commercial reservoir was found. However, between 3.617 and 3.624 it had hydrocarbon evidence. These wells present a metric interbedded sandstones and shales (Fig. 4c).

The 1 CES 111 CE well was drilled in the eastern region of the area on a basement high (Fig. 7c) and volcanic bodies were reported in the cutting samples description. Hydrocarbons were not found, and this well was considered dry. The analysis of drill cuttings indicated that argillites were deposited in deepwater and that they do not characterize typical deposits generated by gravitational flows. They also do not present favorable characteristics for the formation of good reservoirs.

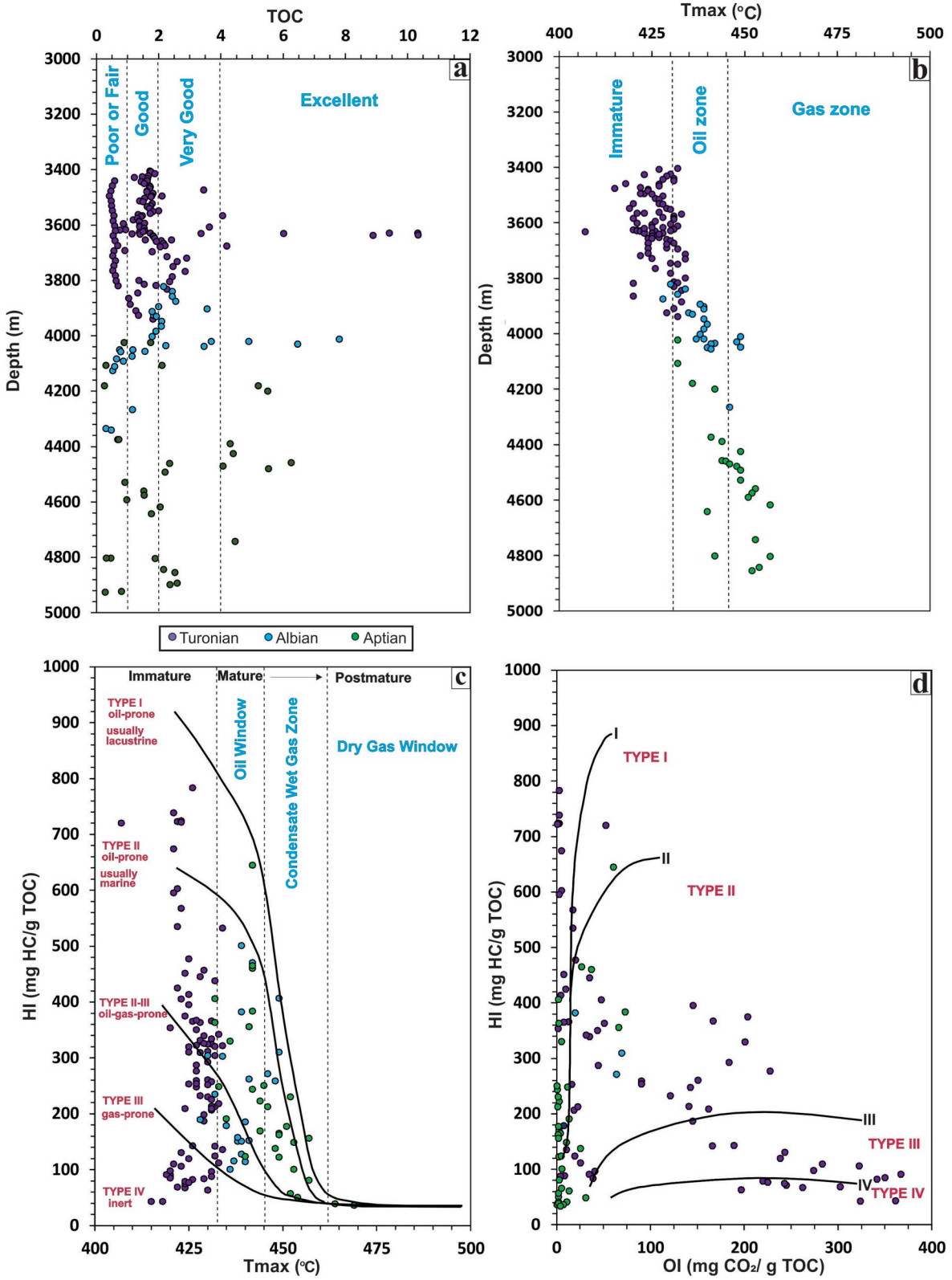

Fig. 12. (a) Plot of total organic carbon (TOC) versus depth showing the source rock generation potential; (b) Tmax versus Depth displaying the maturity of organic matters; (c) Hydrogen Index versus Tmax showing the maturity and the kerogen type; (d) Modified Van Krevelen diagram presenting the primary composition.

However, it should be emphasized that the analysis of electric well data shows that this section is composed of interbedded sandstones and argillites. Apparently, only the argillite sections with more cohesive portions were sampled. Twelve samples were analyzed with the foraminifera method, in order to obtain paleoenvironmental indications. From 2361.60 to 2366.60 m the samples indicate a domination of planktonic forms. These are sometimes well preserved or oxidized in the middle-lower batial environment. From 2485 to 2494 m, the data suggests a dominance of oxidized planktonic forms, with the presence of agglutinating forms of Cyclammina sp. These, although scarce, are

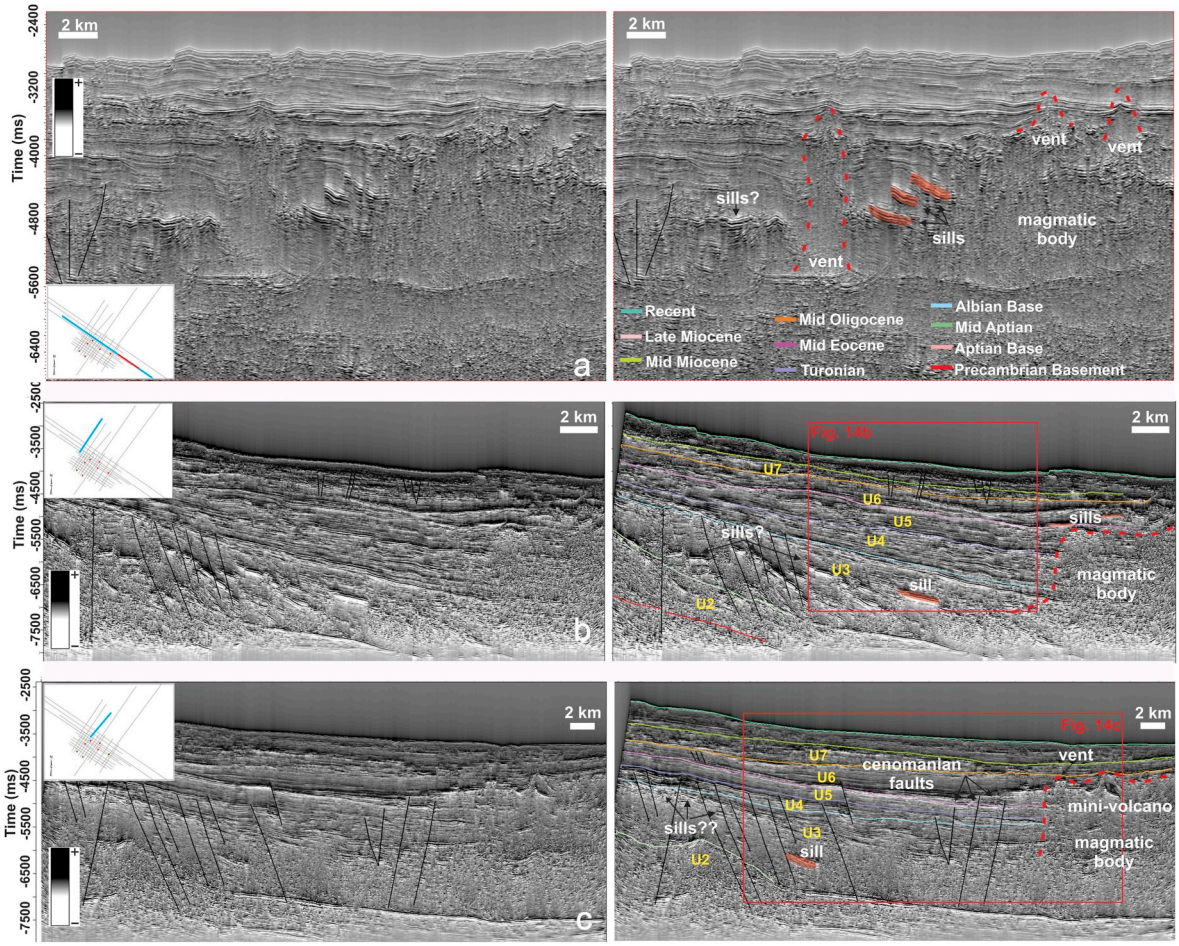

Fig. 13. Seismic lines with stratigraphy uninterpreted and interpreted detailed section showing magmatic bodies. a) NW-SE strike section interpreted showing sills, vents and magmatic bodies; b) SW-NE dip section showing several high-amplitude reflectors associated with sills and a massive magmatic body. Red polygon indicates the area in Fig. 14b; c) SW-NE dip section showing sills, vents, a mini-volcano, and a large magmatic body. Red polygon indicates the area in Fig. 14c. All the magmatic features with the exception of the vents are presented in this area until the late Eocene. (For interpretation of the references to colour in this figure legend, the reader is referred to the Web version of this article.)

also indicative of sedimentation in deeper water environments in the Mid-Miocene age.

Fig. 12a illustrates the values of TOC percentage of rocks from Aptian to Turonian age. Analyzing the last interval, from Early Cenomanian and Cenomanian-Turonian, twenty-six samples presented TOC between 1.0 and 1.5%, with fair potential as source rocks; fifty-seven presented TOC between 1.0 and 2.0%, with a good potential as source rock; eighteen samples presented TOC between 2.0 and 4.0% indicating a very good source rocks; seven samples presented TOC values from 4.0 to up 6% indicating excellent source rocks.

A total of 106 samples from four wells was used for Maximum Temperature (Tmax) analysis (Fig. 12b). Of these, eighty-five samples have Tmax between 400 and 430 °C and are considered immature according to Tissot and Welte (1984), while 21 samples have Tmax values between 430 and 445 °C and are considered to be within the mature zone. Thus, according to well data, the depth of Early Cenomanian and Cenomanian-Turonian source rocks at deepwater of Mundaú-sub basin occurs approximately between 3400 and 3900 m below sea water bottom. At this depth and deeper, there is the additional possibility of oil and gas generation.

On a graph of Hydrogen Index (HI) versus Maximum Temperature (Tmax), seven samples plot within the oil window zone (Fig. 12c). Considering the Hydrogen Index (mgHC/gTOC) versus Oxygen Index (mgCO2/gTOC) of the samples from Albian to Turonian obtained from the recent three wells, it was verified that they have mainly Type II and some samples are Type III organic matter (Fig. 12d). According to Tissot and Welte (1984), Type II organic matter, which is derived from autochthonous marine organic matter deposited in a reducing environment, is favorable to oil and gas generation; while Type III organic matter, which is originated from terrestrial plants, is favorable to gas generation at great depths. Well data analyses support that the drift sequence, characterized by the Ubarana Formation, has a high potential to be a source rock (geochemical graphs) as well as a good reservoir (Fig. 4c-facies).

5.2.1. *Magmatism*

Sill complexes and hydrothermal vents are imaged by numerous high-amplitude reflections primarily within the Cretaceous successions (Figs. 7a, 13 and 14). Hydrothermal vents are characterized by diffuse and irregular seismic features that were identified below the top of the Oligocene unconformity (Fig. 7a). Sills were mapped inside the breakup sequence and in the Unit 6 (Figs. 13 and 14). In the ultra-deepwater, the Unit 6 is almost completely offset by vertical faults related to the reactivation of the Romanche Fracture Zone and emplacement of magmatic bodies (Figs. 5c and 14a). Most of the magma appears to be intrusive, with the exception of the magmatic body imaged in Figure 7b and the Canopus Bank (Figs. 2, 5 and 10).

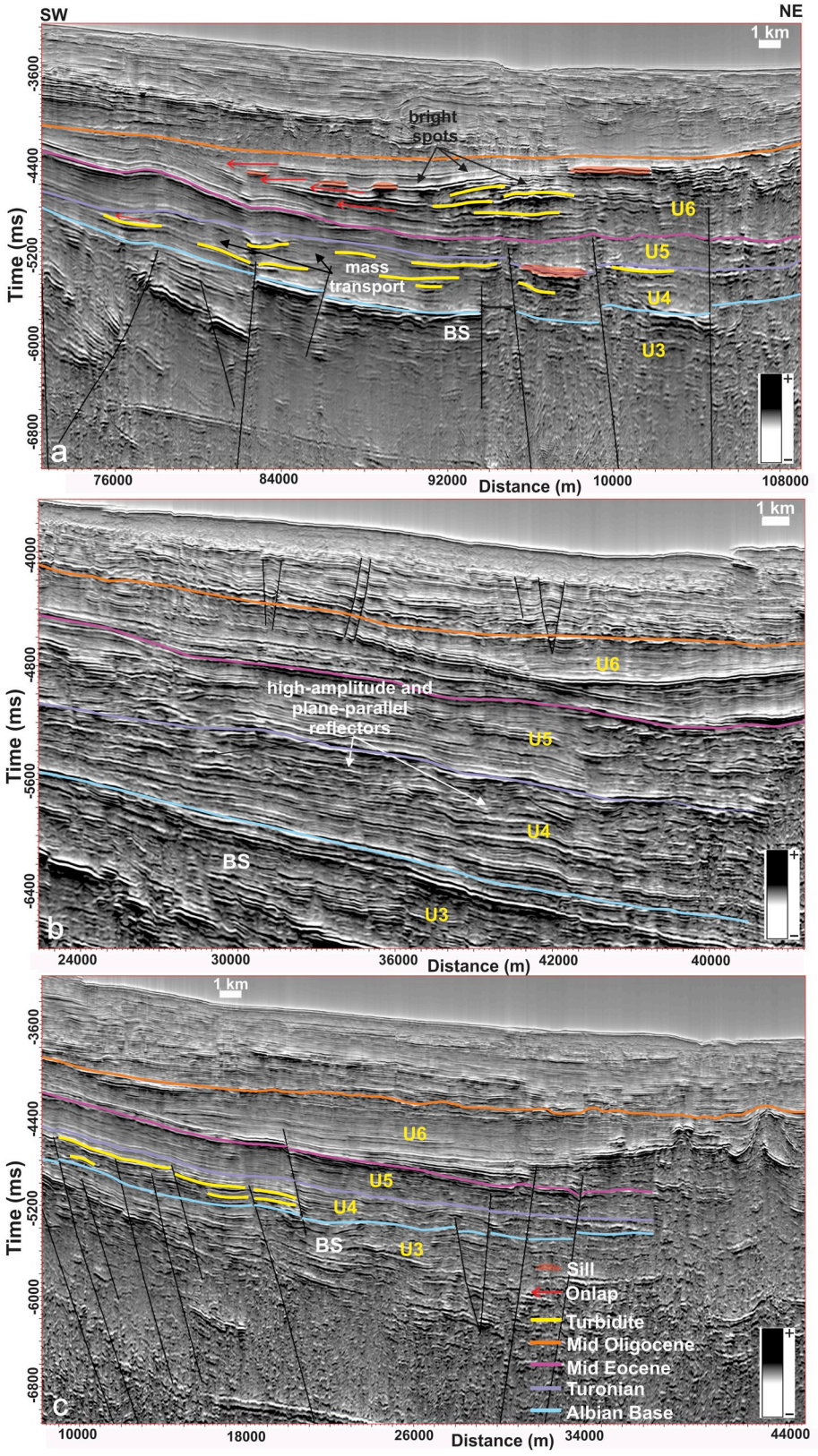

Fig. 14. SW-NE dip seismic lines with stratigraphy uninterpreted and interpreted detailed section showing turbiditic bodies in deepwater. a) Interpreted section showing several bright spots and turbidites of the Late Albian to Turonian possibly saturated with hydrocarbons. These turbidites were interpreted with updip pinch-out and some of them are associated with magmatic bodies. Also, mass-transport are clearly associated with these turbidites. Turbidites from the Late Eocene were also interpreted with updip pinch-out and associated with magmatic bodies (red forms); b) Interpreted section showing several high-amplitude reflectors with patterns probably associated with turbidites of the Late Albian to Turonian; c) Interpreted section showing turbidites of the Late Albian to Turonian. Faults connecting rift, transitional, and drift sequences were interpreted near these turbiditic bodies. This indicates a possible play where the migration occurs directly from rift and transitional source rocks to drift turbiditic reservoir. The seismic section B and C are also shown in a larger view in Fig. 13. (For interpretation of the references to colour in this figure legend, the reader is referred to the Web version of this article.)

6. Discussion

6.1. Basin architecture

6.1.1. Continental shelf segment

The continental shelf segment forms a significant depocenter up to 22 km wide (Fig. 10). This segment is underlain by Precambrian basement, which was cut by NW–SE-trending, planar, high-angle extensional fault systems bounding a series of horst and graben structures infilled by wedge-shaped syn-rift sediments growth strata (units 1 and 2). The thickness reaches up 1200 ms in the central part of the graben (Figs. 5a, 10a and 10b), but accommodation space is related to the main

phase of rifting in the Aptian age. Oceanward-dipping faults are predominant features and the deposition of syn-rift stage was controlled by the border fault that which appears in most of the equatorial margin basins and is well marked by potential field data (Silva Filho et al., 2007). Extensional reactivation of the major faults, and deposition of the breakup sequence (Figs. 5a and 10c), occurred during the earlier Albian and reaches up 800 ms into the central part of the depocenter. Following the end of the rift phase in the upper Aptian, the basin was infilled with a thick (~1700 ms) post-rift sediment sequence during Late Cretaceous–Late Miocene thermal subsidence. All the units described in this work are present in this shelf segment. In addition, the reservoir potential of the rift, breakup and drift sequences within the shelf segment is exemplified by the Curimã, Espada, Xaréu, and Atum fields that are producing in shallow waters.

The greatest thicknesses of drift sediment sequence correspond to Unit 5 on the mini-basin (~800 ms) (Figs. 9e and 11b) and Unit 7 age within three mini-basins (~700 ms) (Figs. 9g and 11d). The period between these two units correspond to Unit 6 (Mid-Eocene to Mid-Oligocene), whose top is related to a major regional unconformity, the "Oligocene unconformity", identified in the Brazilian Equatorial Margin (Condé et al., 2007; Trosdtorf et al., 2007) throughout the west African margin (*e.g.* (Massala et al., 1992; Séranne et al., 1992; McGinnis et al., 1993; Meyers et al., 1996; Rasmussen, 1996; Mauduit et al., 1997; Nzé Abeigne, 1997; Karner and Driscoll, 1999; Mougamba, 1999; Séranne and Nzé Abeigne, 1999; Cramez and Jackson, 2000; Lavier et al., 2000), and Eastern Margins of Brazil (Rossetti et al., 2013).

6.1.2. Slope segment

Landward-dipping faults are a predominant feature in this part of the basin and are in contrast to non-volcanic margins, in which the oceanward-dipping faults are a major tectonic feature (Abreu, 1998). These landward-dipping faults affected the outer edge of the continental crust. The slope developed structures of horsts and grabens formed under the control of extensional landward-dipping faults, contrast with the orientation of the ones within the continental shelf. The structural maps of the Basement, Aptian base and Mid Aptian horizons document the presence of a well-developed, NW–SE-trending extensional fault system. Four majors NW-SE faults were mapped in the seismic data set (Figs. 5–7). This segment has well-developed rifted strata and depression strata with depocenter thickness over 2640 ms (Figs. 5b, 10a and 10b). Mello et al. (1994) presented that in the Equatorial Atlantic the most important deepwater petroleum source rocks are associated with deeply buried syn-rift sediments. Seismic facies of units 1 and 2 reveal wedge/lens strong reflection configurations indicating syn-rift deposition. The main depocenters of Unit 1 are up to 2000 ms thick, are located along the syn-rift hanging wall faults. The assumption of older rocks from Barremian or Jurassic ages is not disregarded due to the fact of the great thickness of these unit and the presence of the sedimentary column from these ages in the conjugated margin (Elvsborg and Dalode, 1985; Brownfield and Charpentier, 2006). The Mundaú Fm. presents anticline structures caused by high dip faults and flower structures (Fig. 5b). The deposition of syn-rift sequence ends in the toe of the slope segment when the proto-oceanic crust begins to form (Figs. 5b and 10a).

The breakup sequence (Unit 3) has a greater thickness in relation to the syn-rift sequences as the continental crust is transforming to oceanic crust (Fig. 10b) (Soares et al., 2012). In comparison with syn-rift deposition, the drift deposition (Units 4 to 9) has a less representative thickness demonstrating the basin dynamics of erosion and deposition during its development (Fig. 10d). Seismic data reveals a contrast of the structural styles of the intervals deposited above and below the Paracuru Formation (Figs. 5–7). The structural framework of basement and syn-rift sequences is characterized by the presence of large antithetic normal faults, which were formed during the rift stage of the Brazilian equatorial margin and persisted until end of Albian (Pellegrini and Ribeiro, 2018). The structural framework of drift sequences is characterized by synthetic and antithetic small faults, from upper Cenomanian to later Eocene ages, which occur mainly in the slope (Fig. 5b). This same type of fault also occurs in the Barreirinhas Basin (Pellegrini and Ribeiro, 2018).

6.1.3. Deepwater segment and magmatism

High-angle faults and flower structures are a predominant feature in this part of the basin as well as bodies related to magmatism: sills and vents (Figs. 5c and 14a). These faults probably developed and deformed the sediments of the drift stage by reactivation of breakup faults, as its approaches the Romanche Fracture Zone (Fig. 1b). The transitional sequence has a thicker sedimentary distribution in this region and the drift sedimentary infilling has, in general, parallel to sub-parallel seismic reflection patterns. The detailed interpretation of the sedimentary fill reveals a considerable depocenter of drift sequences (2300 ms thick) (Figs. 5c, 10a and 10d). A thicker sedimentary overburden is the ideal site for the maturation of the Late Albian to Turonian source rocks present at the base of the drift sequences. Inside this depocenter, a few bright spots associated to updip pinch-out are clearly visible (Fig. 14a). Such depositional geometries are typical of turbidite bodies saturated with hydrocarbons; some are trapped in mixed stratigraphic-structural traps by possible sills bodies. These plays are very similar to the basin's African counterpart, with exception of the turbidites mixed by sills bodies that consists in an atypical play. All of them, point to hydrocarbon potential in the Mundaú sub-basin.

Sill complexes and hydrothermal vents imaged by seismic lines in the distal Mundau sub-basin are similar in style and position to the sills observed in the Cretaceous–Paleocene sediments of the others volcanic margins basins (e.g. Skogseid and Eldholm, 1989; Skogseid et al., 1992, Larsen and Marcussen, 1992). It is no possible to decipher the exact age of the magmatism in the deepwater because there are no geochronological data over these features. Only a few magmatic rocks were recovered in the 1 CES 111 CE well into Unit 5 (Fig. 4c), however, this well does not reached the breakup and rift sequences. Based on the seismic-stratigraphic interpretation, we suggest that this magmatism most probably related to a syn-rift phase (pre-break-up) event, and a reactivation event until Early Oligocene. In the eastern part of the BEM, within the Potiguar Basin, magmatic events are interpreted to have occurred during the syn-rift phase (Fonseca et al., 2019).

We propose that the architecture of this basin is best classified as a volcanic margin. Volcanic rifted margins and continental flood basalts are among the Largest Igneous Provinces (LIP) on Earth (Abreu, 1998). Examples of conjugate volcanic rifted margins in the South Atlantic Ocean are Pelotas (Brazil) and Walvis (Namibia) basins. Zálan (2015) classified the Mundaú sub-basin and Potiguar basin as transitional passive margins and the onshore rift of Potiguar Basin as volcanic passive margin. However, strong evidence points out that this margin can be considered volcanic: (1) the presence of basement and rifts filled by seaward dipping reflectors; (2) the COB is placed where the SDRs abut against the tabular body of oceanic crust, and (3) absence of exhumed mantle between the continental crust and oceanic crust. In addition, Hollanda et al. (2018) recognized a Cretaceous LIP in South America, known as the Equatorial Atlantic Magmatic Province (EQUAMP), owing to the fact that magmatic products of the Sardinha Formation and Rio Ceará-Mirim Group were found over an area of about 700,000 km^2 in the neighboring basins. In addition, Leopoldino Oliveira et al. (2018) show evidence of volcanic bodies (dykes) near coastlines in the Potiguar Basin imaged by potential field methods.

6.2. Implications for the petroleum potential

6.2.1. Magmatism

Senger et al. (2017) explained about the effects of igneous intrusions on the petroleum system. Magmatic activity has, mostly through improved source rock maturation and compartmentalization, performed a key role in the petroleum systems of many basins including the

onshore-offshore Taranaki Basin in New Zealand (Stagpoole and Funnell, 2001), the Faroe-Shetland and Rockall Trough Basins in the North Atlantic (Rohrman, 2007; Schofield et al., 2015), the Møre-Vøring basins offshore mid-Norway (Aarnes et al., 2015), the Sverdrup Basin of Arctic Canada (Jones et al., 2007), the Siberian Tunguska Basin (Svensen et al., 2009) and the Brazilian basins such as the Parnaiba basin (Miranda et al., 2016). The potential regional impact of igneous intrusions on hydrocarbon migration has been well documented in Western Australia (Holford et al., 2013) and the Brazilian basins (Thomaz Filho et al., 2008).In fact, igneous intrusions may both create new migration pathways if they are fractured and permeable, or they can act as fluid flow barriers if they are mineralized and impermeable. Also, igneous intrusions may form hydrocarbon traps directly and indirectly. Similarly, to sealing faults, impermeable intrusions such as dykes, sills, and vents cross-cutting stratigraphy, may generate numerous traps for migrating hydrocarbons (Senger et al., 2017). Besides, most igneous intrusions that are not fractured and altered are impermeable and hence may act as a good sealing rocks (e.g., Wu et al., 2006). In addition, non-altered intrusions may behave as a lateral and top seal for hydrocarbon accumulations (Thomaz Filho et al., 2008).

The deepwater of Mundau sub-basin presents igneous intrusions from Cretaceous to Paleogene strata. This differs from the shallow water region where magmatism occurred between the Mid-Eocene and Lower Oligocene, but with local samples of Santonian-Turonian age (Mizusaki et al., 2002; Condé et al., 2007). Maia de Almeida et al. (2019) also observed a magmatic intrusion inside the breakup sequence in the deepwater domain (Unit 3). Due to large presence of igneous features in the deepwater segment of the Mundaú sub-basin, an atypical petroleum system can exist there. For hydrocarbon generation, magma intrusions are responsible for the increase in temperature in the system and consequent maturation of the organic matter. As seen in Fig. 12a the drift stage, Turonian age samples, has immature sequences with a good and excellent TOC potential. Regarding the oil migration, if those intrusions are fractured and have permeability, they will act as a migration route, if they are impermeable, they will form a structural trap preventing the passage of fluids. Fig. 14a presents turbiditic bodies from Oligocene age with a clear proximity of sills that may act as seals. Furthermore, the mapping of this igneous activity is important also to E &P activities since they can represent drilling risks.

6.2.2. Rift-drift structural trap opportunity

The presence of a well-developed rift architecture in the deepwater Ceará Basin (Figs. 5–7) provides further opportunities for structural trapping in the basin and expectations of post-rift stratigraphic traps, as in the African counterpart (Macgregor et al., 2003; Dailly et al., 2013; Scarselli et al., 2018). In Ghana, the hydrocarbons would have accumulated mostly in structural traps afforded by the widespread rotated fault blocks associated with the rifted basins and half-graben (Antobreh et al., 2009). Maia de Almeida et al. (2019) compared the petroleum system in shallow water and deepwater of Mundau sub-basin and suggested that an importance source interval can exist in the initial syn-rift sequence. Thus, the numerous interconnecting Cenomanian faults would have the potential to allow charging of deepwater post-rift reservoirs from rift sources. (Figs. 5–7). Early drift stage reservoirs have been found to be of good quality based on well data from the continental shelf of the Ceará Basin (Condé et al., 2007) and Côte d'Ivoire margin (Macgregor et al., 2003). Additional post-rift hydrocarbon charge may come from Cenomanian source rocks on the equatorial margin (Morrison et al., 2000; Macgregor et al., 2003; Dailly et al., 2013). Recent exploration efforts have documented the presence of high-quality Upper Cretaceous turbidite reservoirs in the inner slope offshore Ghana (Jubilee field) and Côte d'Ivoire (Paon discovery; Dailly et al., 2013; Coole et al., 2015; Martin et al., 2015). Detailed seismic analysis and drilling have indicated that these reservoirs extend into the deepwater of the Ivorian Tano Basin (Martin et al., 2015).

6.2.3. Turbidite play

According to Maia de Almeida et al. (2019), based only in the 1 BRSA 1080 CES well, the source rocks of Ubarana Formation was considered immature, although its excellent TOC values. The authors also described that gas was found in this formation in reservoirs with hyaline sandstones intercalated to greenish dark to light shales, and it was migrated from transitional source rocks along faults. As described in the well data results, oil was found in Ubarana Formation in the 1 BRSA 1114 CES and 1 BRSA 1150 CES wells with 40 °API, however no commercial quantity. Also, the interval between Albian base to Turonian age has a good percentage of sandstones and shales as demonstrated by Vsh and facies log (Fig. 4a and c), and from rock samples in these wells.

According to Veeken (2007), the configuration and nature of basin infill are affected by factors such as tectonic subsidence, input of sediment supply, morphology of the substratum, eustatic sea level changes, base-level profile, and climatic conditions. In the deepwater of the Mundaú sub-basin, based on seismic interpretation, the drift deposits were mainly influenced by sediment input from the continental shelf and slope instabilities (e.g. canyons and slumps in Figs. 7 and 11) and volcanic emplacement represented by sills, mini-volcano, and hydrothermal vents (Figs. 7, 13 and 14). The deepwater Ubarana Formation from Albian to Turonian age consists primarily of turbidites and has potential as a hydrocarbon play (as shown in Figs. 14 and 15). In this region, the main control on the distribution of turbiditic sands is the post-rift seabed geomorphology that were occasionally affected by sills intrusion (Figs. 7, 11, 13 and 14). These features could develop highs that would form structures against which sands would onlap and pinch out, creating the potential for accumulation of reservoirs and opportunity for stratigraphic traps to develop (Fig. 14a). These turbidites are extensive and are commonly associated with mass transport deposits, which is also seen in the east Brazilian margin (e.g. Fiduk et al., 2004; Mohriak, 2005; Gamboa et al., 2010). The interpreted turbiditic sandstones have reflectors with high acoustic impedance contrasts, low frequency, lens external geometry, and variable lateral extension, ranging from 5 to 8 km (Figs. 14 and 15).

There are two possible source rocks for this play: the marine shales of the Aptian Paracuru Formation, and the marine shales of the Late Albian-Early Cenomanian Ubarana Formation. In the first case, the hydrocarbons generated by shales of Paracuru Formation migrated through Cenomanian faults and unconformity traps. In the second case, the hydrocarbons generated by marine shales of the Ubarana Formation migrate directly from source rock to reservoir. The seal rocks are the shales of the Ubarana Formation itself, and stratigraphic traps were created by as depositional pinch-out and structure formed by volcanic bodies.

Based on the geochemical data, the depth of Early Cenomanian and Cenomanian-Turonian source rocks at deepwater of Mundaú sub-basin occurs approximately between 3400 and 3800 m below sea water bottom. Also, the depth of source rocks from Late Albian-Early Cenomanian and Cenomanian-Turonian is approximately from 3048 to 4894 m in the deepwater and ultra-deepwater based on the conversion of time to depth. Thus, it can be inferred that source rocks of the drift stage from deepwater's Mundaú sub-basin are at the oil window depth, since the source rocks reached the burial depth greater than 3400 m below the sea floor. Unit 4 (Figs. 9d and 11a) reveals the most likely areas of deepwater turbiditic deposits in the Mundaú sub-basin, which corresponds to Late Albian-Turonian ages, an analogue to the play found in the Jubilee field offshore Ghana.

7. Conclusions

New well data combined with 1,589 km of 2D seismic lines allowed for a new geological evaluation of the deepwater stratigraphy of Ceará Basin and its architectural framework. In this study, new insights were presented on the influence of structural features on the depositional

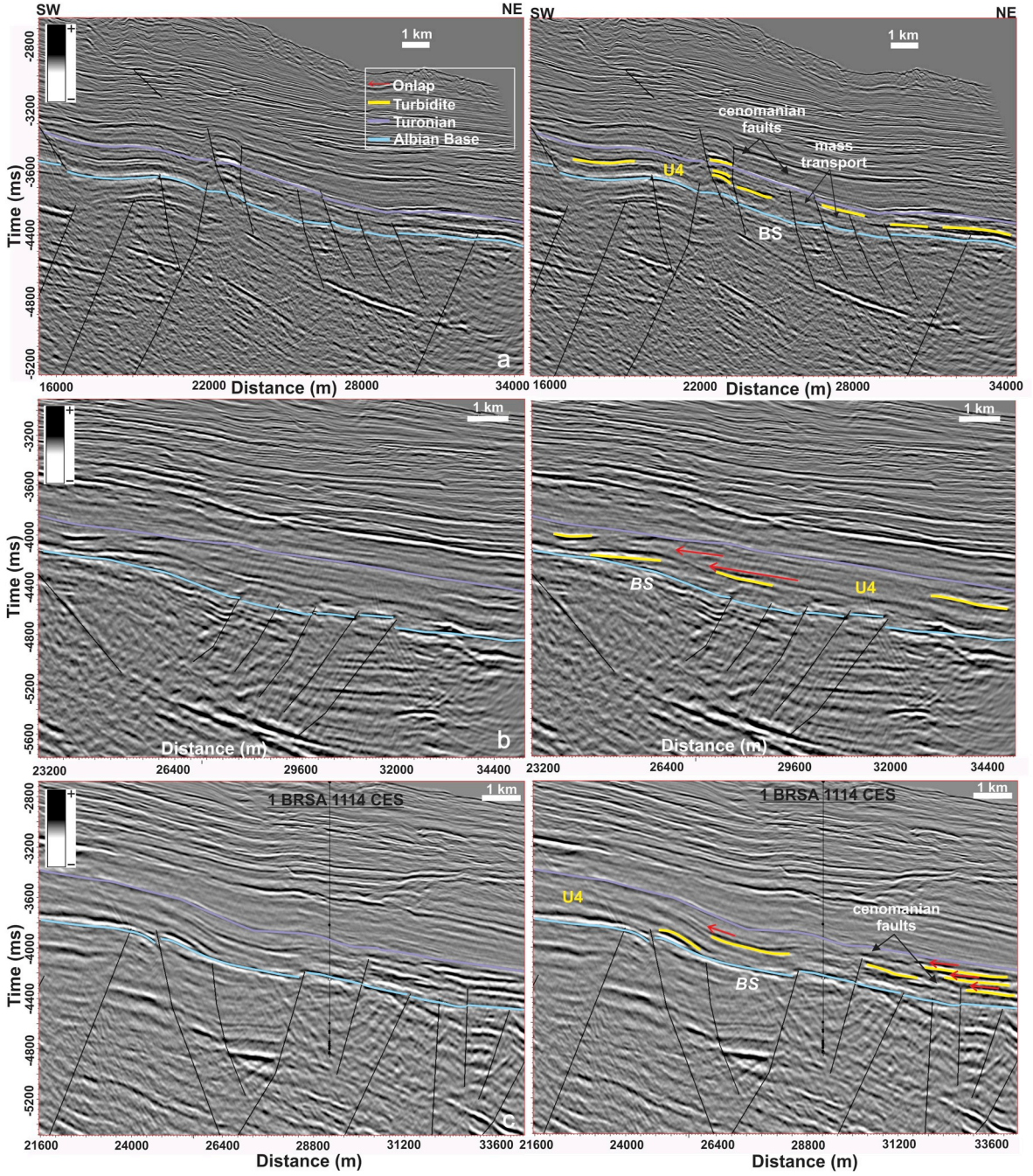

Fig. 15. SW-NE oriented seismic lines with stratigraphy uninterpreted and interpreted detailed section showing turbiditic bodies in deepwater. a) Interpreted section showing turbidites of the Late Albian to Turonian age. Faults connecting rift, transitional, and drift sequences were interpreted near these turbiditic bodies. This indicates a possible play where the migration occurs directly from the rift and transitional source rocks to drift turbiditic reservoir; b) Interpreted section showing turbidites of the Late Albian to Turonian where updip pinch-out was interpreted. These reflector patterns show interbedding of turbidite and shales; c) Interpreted section displaying turbidites of the Late Albian to Turonian with updip pinch-out. Faults connecting rift, transitional, and drift sequences were interpreted near these turbiditic bodies. This indicating a possible play where the migration occurs directly from the rift and transitional source rocks to drift turbiditic reservoir. The 1 BRSA 1114 well and its hydrocarbon evidence are labeled (black dots).

elements and their distribution. The interplay between sedimentation and tectonics plays a key role in controlling sediment trapping and spatial distribution as well as the petroleum implications of this region. The following observations and interpretations have been made:

(1) The Aptian rift system in Mundaú sub-basin might supply further opportunities for structural trapping in the basin, and expectations of drift stratigraphic-structural traps through interconnecting faults. Four majors landward-dipping faults were mapped in all seismic data, which would have the potential to allow charging of deep-water drift reservoirs from rift source rocks.
(2) The seismic interpretation reveals evidence of Cretaceous to Paleocene magmatism in the region as indicated by the well imaged volcanoes and associated sills at depth. The proximity of deepwater turbidites plays with magmatic rocks could have established an atypical petroleum system.
(3) The variety of stratigraphic and structural features developed through the Cretaceous history of the basin offer high-trapping

potential for a number of plays in the rift as well as in the drift sequences. The type of plays are: (1) the developed rift system with major faults which can act as long-distance migration pathways; (2) turbiditic bodies; (3) turbiditic bodies associated with magmatic intrusion. Identification of potential plays associated with turbiditic sandstones of the Ubarana Formation can be correlated to Jubilee play in Guinea Gulf and Zaedyus play in French Guiana.

(4) The sediments from Late Albian-Early Cenomanian-Turonian age are at depths ranging from 3048 to 4894 m in the deepwater and ultra-deepwater domains. Since the top depth of the oil window occurs from about 3400 to 3800 m in the deepwater Mundaú sub-basin, the analyses of geochemical data suggest that in this basin there must be generation of oil and/or gas at deepwater plays.

(5) Our data strongly suggest that the architecture of this basin is a volcanic passive margin. Volcanic passive margins are associated with the extrusion and intrusion of large volumes of magma, predominantly mafic, and represent distinctive features of Larges Igneous Provinces, in which regional fissural volcanism predates localized syn-magmatic break-up of the lithosphere. The criteria used to justify our assertion are: (1) the presence of basement and rifts filled by volcanics (seaward dipping reflectors); (2) the absence of exhumed mantle between the continental crust and oceanic crust; (3) the large presence of igneous intrusions; (4) and the presence of a LIP in the equatorial margin, based on igneous intrusions between two basins near the Ceará Basin.

CRediT authorship contribution statement

Karen M. Leopoldino Oliveira: Conceptualization, Data curation, Formal analysis, Investigation, Methodology, Validation, Visualization, Writing - original draft, Writing - review & editing. **Heather Bedle:** Resources, Supervision, Visualization, Writing - original draft, Writing - review & editing. **R. Mariano G. Castelo Branco:** Project administration, Resources, Supervision, Writing - review & editing. **Ana Clara B. de Souza:** Visualization, Formal analysis, Writing - review & editing. **Francisco Nepomuceno Filho:** Project administration, Resources, Supervision, Writing - review & editing. **Márcio N. Normando:** Writing - review & editing. **Narelle M. de Almeida:** Writing - review & editing. **Thiago H. da Silva Barbosa:** Writing - review & editing.

Declaration of competing interest

The authors declare that they have no known competing financial interests or personal relationships that could have appeared to influence the work reported in this paper.

Acknowledgements

The authors are grateful to the Brazilian National Petroleum Agency (ANP) for the provision of seismic and well data, and to Schlumberger for software licenses. The first author also thanks to Federal University of Ceará (LGPSR – Laboratório de Geofísica de Prospecção e Sensoriamento Remoto, and LSBD – Laboratório de Sistemas e Banco de Dados) for their support to this study. CImaGeo is also acknowledged for their support in seismic processing. The first author is grateful to the Fulbright Commission Brazil for a grant to support in her research in the United States. KMLO thanks the School of Geosciences, the University of Oklahoma, for providing facilities during her split PhD in the United States. This study was financed in part by the Coordenação de Aperfeiçoamento de Pessoal de Nível Superior - Brasil (CAPES) - Finance Code 001. We are also grateful to Davide Gamboa and to an anonymous reviewer for their constructive discussion and comments, and also the editor Tiago Alves for their help in improving the quality of the original manuscript.

References

Aarnes, I., Planke, S., Trulsvik, M., Svensen, H., 2015. Contact metamorphism and thermogenic gas generation in the Vøring and Møre basins, offshore Norway, during the Paleocene-Eocene thermal maximum. J. Geol. Soc. 172 (5), 588–598. https://doi.org/10.1144/jgs2014-098.

Abreu, V.S., 1998. Geologic Evolution of Conjugate Volcanic Passive Margins: Pelotas Basin (Brazil) and Offshore Namibia (Africa). Implication for Global Sea Level Changes. Diss., Rice University. https://hdl.handle.net/1911/19338.

Altamira-Areyan, A., 2009. The Ribbon Continent of Northwestern South America. Ph.D. Dissertation. University of Houston, pp. 215.

Antobreh, A., Faleide, J., Tsikalas, F., Planke, S., 2009. Rift–shear architecture and tectonic development of the Ghana margin deduced from multichannel seismic reflection and potential field data. Mar. Petrol. Geol. 26 (3), 345–368. https://doi.org/10.1016/j.marpetgeo.2008.04.005.

Antunes, A.F., Jardim de Sá, E.F., Araújo, R.G.S., Lima Neto, F.F., 2008. Caracterização tectonoestrutural do Campo de Xaréu (Sub-Bacia de Mundaú, Bacia do Ceará – NE do Brasil): abordagem multiescala e pluriferramental. Rev. Bras. Geociencias 38 (1 - Suppl. o), 88–105.

Beltrami, C.V., Alves, L.E.M., Feijó, F.J., 1994. Bacia do. Ceará. B. Geoci. Petrobras 8 (1), 117–125.

Bishop, M.S., 1960. Surface Mapping. John Willey, New York, pp. 198.

Bulhões, E.M., Amorim, W.N., 2005. Princípio da sismocamada elementar e sua aplicação à técnica de volume de amplitudes (TecVa): Ninth International Congress of the Brazilian Geophysical Society, Salvador, Brasil. https://doi.org/10.1190/sbgf2005-275.

Burov, E., Cloetingh, S., 1997. Erosion and rift dynamics: new thermomechanical aspects of post-rift evolution of extensional basins. Earth Planet Sci. Lett. 150, 7–26. https://doi.org/10.1016/S0012-821X(97)00069-1.

Burov, E., Poliakov, A., 2003. Erosional forcing of basin dynamics: new aspects of syn-and post-rift evolution. In: In: NIEUWLAND, D.A. (Ed.), New Insights into Structural Interpretation and Modelling, vol. 212. Geological Society, London, Special Publications, pp. 209–223. https://doi.org/10.1144/GSL.SP.2003.212.01.14.

Brownfield, M.E., Charpentier, R.R., 2006. Geology and Total Petroleum Systems of the Gulf of Guinea Province of West Africa: U.S. Geological Survey Bulletin 2207-C, pp. 32.

Condé, V.C., Lana, C.C., Pessoa Neto, O.C., Roesner, E.H., Morais Neto, J.M., Dutra, D.C., 2007. Bacia do. Ceará. B. Geoci. Petrobras 15 (2), 347–355.

Coole, P., Tyrrell, M., Roche, C., 2015. Offshore Ivory Coast: reducing exploration risk. GeoExpro 12, 80–84.

Costa, I.G., Beltrami, C.V., Alves, L.E.M., 1990. A Evolução tectono-sedimentar e o "habitat" do óleo na Bacia do Ceará. Bol. Geociencias Petrobras 12 (1), 65–74.

Cramez, C., Jackson, M.P.A., 2000. Superposed deformation straddling the continental oceanic transition in deepwater Angola. Mar. Petrol. Geol. 17, 1095–1109. https://doi.org/10.1016/S0264-8172(00)00053-2.

Dailly, P., Henderson, T., Hudgens, E., Kanschat, K., Lowry, P., 2013. Exploration for cretaceous stratigraphic traps in the Gulf of Guinea, west Africa and the discovery of the jubilee field: a play opening discovery in the Tano Basin, offshore Ghana. In: In: Mohriak, W.U., Danforth, A., Post, P.J., Brown, D.E., Tari, G.C., Nemčok, M., Sinha, S.T. (Eds.), Conjugate Divergent Margins, vol. 369. Geological Society, London, Special Publications, pp. 235–248. https://doi.org/10.1144/SP369.12.

Davison, I., Faull, T., Greenhalgh, J., Beirne, E.O., Steel, I., 2016. Transpressional structures and hydrocarbon potential along the Romanche Fracture Zone: a review. In: In: Nemčok, M., Rybár, S., Sinha, S.T., Hermeston, S.A., Ledvényiová, L. (Eds.), Transform Margins: Development, Controls and Petroleum Systems: London, vol. 431. Geological Society, Special Publications, pp. 235–248.

Elvsborg, A., Dalode, J., 1985. Benin hydrocarbon potential looks promising. Oil Gas J. 82, 126–131.

Falkenhein, F., Martins Neto, M., Guerra, W.J., 2001. Brazilian Equatorial Margin Project Part. 1: Final Report. Brazilian National Agency of Petroleum, Natural Gas and Biofuels Internal Report.

Fiduk, J.C., Brush, E.R., Anderson, L.E., Gibbs, P.B., Rowan, M.G., 2004. Salt deformation, magmatism, and hydrocarbon prospectivity in the Espírito Santo Basin, offshore Brazil. In: Post, P.J., Olson, D.L., Lyons, K.T., Palmes, S.L., Harison, P.F., Rosen, N.C. (Eds.), Salt-sediment Interactions and Hydrocarbon Prospectivity: Concepts, Applications, and Case Studies for the 21st Century. GCSSEPM 24th Annual Research Conference, pp. 370–392.

Fonseca, J.C.L.G., Vital, H., Perez, Y.A.R., et al., 2019. Seismic stratigraphy of a deep water basin in the Brazilian equatorial margin: the eastern portion of Potiguar Basin and Touros High. Geo Mar. Lett. https://doi.org/10.1007/s00367-019-00626-7.

Françolin, J.B.L., Szatmari, P., 1987. Mecanismo de rifteamento da porção oriental da margem norte brasileira. Rev. Bras. Geociencias 17 (2), 196–207.

Gamboa, D., Alves, T.M., Cartwright, J., Terrinha, P., 2010. MTD distribution on a 'passive' continental margin: the Espírito Santo Basin (SE Brazil) during the Palaeogene. Mar. Petrol. Geol. 27 (7), 1311–1324. https://doi.org/10.1016/j.marpetgeo.2010.05.008.

Haq, B.U., Hardenbol, J., Vail, P.R., 1987. Chronology of fluctuating sea levels since the Triassic (250 million years ago to present). Science 235, 1156–1167. https://doi.org/10.1126/science.235.4793.1156.

Holford, S., Schofield, N., Jackson, C., Magee, C., Green, P., Duddy, I., 2013. Impacts of igneous intrusions on source and reservoir potential in prospective sedimentary basins along the western australian continental margin, West Australian Basins Symposium, Abstracts. http://hdl.handle.net/10044/1/32040.

Hollanda, M.H.B.M., Archanjo, C.J., Macedo Filho, A.A., Fossen, H., Ernst, R.E., de Castro, D.L., Melo, A.C., Oliveira, A.L., 2018. The Mesozoic Equatorial Atlantic Magmatic

Province (EQUAMP) A New Large Igneous Province in South America. Springer Geology Book Series: Dyke Swarms of the World: A Modern Perspective, pp. 87–110. https://doi.org/10.1007/978-981-13-1666-1_3.
Jones, S.F., Wielens, H., Williamson, M.C., Zentilli, M., 2007. Impact of magmatism on petroleum systems in the Sverdrup basin, Canadian Arctic islands, Nunavut: a numerical modelling study. J. Petrol. Geol. 30 (3), 237–256.
Jovane, L., Picanco Figueiredo, J., Pavani Alves, D., Iacopini, D., Giorgioni, M., Vannucchi, P., Silva de Moura, D., Hilario Bezerra, F., Vital, H., Rios, I., Molina, C., E, 2016. Seismostratigraphy of the Ceará plateau: clues to decipher the cenozoic evolution of Brazilian equatorial margin. Front. Earth Sci. 4, 90. https://doi.org/10.3389/feart.2016.00090.
Karagiannopoulos, L., 2018. Ghana's First Oil Exploration Licensing Round Attracts Global Majors. Dec 24. Reuters. https://www.reuters.com/article/us-ghana-oil-exploration/ghanas-first-oil-exploration-licensing-round-attracts-global-majors-idUSKCN1ON0XQ, Accessed date: 28 April 2019.
Karner, G.D., Driscoll, N.W., 1999. Tectonic and stratigraphic development of the West African and eastern Brazilian Margins: insights from quantitative basin modelling. In: Cameron, N.R., Bate, R.H., Clure, V.S. (Eds.), The Oil and Gas Habitats of the South Atlantic. Geological Society, London, pp. 11–40. https://doi.org/10.1144/GSL.SP.1999.153.01.02.
Krueger, A., 2012. The Brazilian Equatorial Margin from Rift to Drift: Faulting, Deposition, and Deformation in the Offshore Barreirinhas Basin. Ph.D. Dissertation. University of Houston, pp. 168p.
Krueger, A., Murphy, M., Burke, K., Gilbert, E., 2014. The Brazilian Equatorial Margin: A Snapshot in Time of an Oblique Rifted Margin: Adapted from Extended Abstract Prepared in Conjunction with Oral Presentation at AAPG 2014 Annual Convention and Exhibition, Houston, Texas, April 6-9. Search and Discovery Article #30325. http://www.searchanddiscovery.
Larsen, H.C., Marcussen, C., 1992. Sill-intrusion, flood basalt emplacement and deep crustal structure of the Scoresby Sund region, east Greenland. In: In: Storey, B.C., Alabaster, T., Pankhurst, R.J. (Eds.), Magmatism and the Causes of Continental Break-Up, vol. 68. Geological Society, London, Special Publications, pp. 365–386. https://doi.org/10.1144/GSL.SP.1992. 068.01.23.
Lavier, L., Steckler, M., Brigaud, F., 2000. An improved method for reconstructing the stratigraphy and bathymetry of continental margins: application to the cenozoic tectonic and sedimentary history of the Congo margin. AAPG Bull. 84 (7), 923–939. https://doi.org/10.1306/A9673B6C-1738-11D7-8645000102C1865D.
Leopoldino Oliveira, K.M., De Castro, D.L., Castelo Branco, R.M.G., De Oliveira, D.C., Alvite, E.N.C., Jucá, C.C.A., Castelo Branco, J.L., 2018. Architectural framework of the NW border of the onshore Potiguar Basin (NE Brazil): an aeromagnetic and gravity based approach. J. S. Am. Earth Sci. 8, 700–714. https://doi.org/10.1016/j.jsames.2018.10.002.
Macgregor, D.S., Robinson, J., Spear, G., 2003. Play fairways of the Gulf of Guinea transform margin. In: In: Arthur, T.J., Macgregor, D.S., Cameron, N.R. (Eds.), Petroleum Geology of Africa: New Themes and Developing Technologies, vol. 207. Geological Society, London, Special Publications, pp. 131–150. https://doi.org/10.1144/GSL.SP.2003.207.7.
Maia de Almeida, N., Alves, T.M., Nepomuceno Filho, F., Satander Sá Freire, G., Braga de Souza, A.C., Nunes Normando, M., et al., 2019. Tectono-sedimentary evolution and petroleum systems of Mundaú Sub-Basin: a new deep-water exploration frontier in equatorial Brazil, (in press; preliminary version published online Ahead of Print 01 August 2019). AAPG (Am. Assoc. Pet. Geol.) Bull. https://doi.org/10.1306/07151917381.
Martin, J., Duval, G., Lamourette, L., 2015. What lies beneath the deepwater tano basin. GeoExpro 12, 28–30.
Massala, A., de Klasz, I., de Klasz, S., Laurin, B., 1992. translated: benthic foraminifera of stratigraphic interest from the Congo Basin. In: Curnelle, R. (Ed.), African Geology; First Meeting on the Stratigraphy and Paleogeography of West Africa Sedimentary Basins; Second African Meeting on Micropaleontology. Elf-Aquitaine Research Centre, pp. 411.
Matos, R.M.D., 1999. Tectonic evolution of the Equatorial South Atlantic. In: In: Mohriak, W.U., Talwani, M. (Eds.), Atlantic Rifts and Continental Margins, vol. 115. AGU Geophysical Monograph, pp. 331–354. https://doi.org/10.1029/GM115p0331.
Matos, R.M.D., 2000. Tectonic evolution of the Equatorial South Atlantic. In: In: Mohriak, W.U., Talwani, M. (Eds.), Atlantic Rifts and Continental Margins: Geophysical Monograph, vol. 115. pp. 331–354 (AGU).
Mauduit, T., Guerin, G., Brun, J.P., Lecanu, H., 1997. Raft tectonics: effects of basal slope angle and sedimentation rate on progressive extension. J. Struct. Geol. 19 (9), 1219–1230. https://doi.org/10.1016/S0191-8141(97)00037-0.
McGinnis, J.P., Driscoll, N.W., Karner, G.D., Brumbaugh, W.D., Cameron, N., 1993. Flexural response of passive margins to deep-sea erosion and slope retreat: implications for relative sea-level change. Geology 21, 893–896. https://doi.org/10.1130/0091-7613(1993)021%3C0893:FROPMT%3E2.3.CO;2.
McHone, J.G., 2006. Igneous features and geodynamic models of rifting and magmatism around the Central Atlantic Ocean. Available online at: http://www.mantleplumes.org/CAMP.html.
Mello, M.R., Mohriak, W.U., Koutsoukos, E.A.M., Bacoccoli, G., 1994. Selected petroleum systems in Brazil. AAPG Memoir 60, 499–512.
Meyers, J.B., Rosendahl, B.R., Austin, J.A.J., 1996. Deep-penetrating MCS images of the South Gabon Basin: implications for rift tectonics and post-breakup salt remobilization. Basin Res. 8, 65–84. https://doi.org/10.1111/j.1365-2117.1996.tb00115.x.
Milani, E.J., Thomaz Filho, A., 2000. Sedimentary basins of South America. In: In: Cordani, U.G., Milani, E.J., Thomaz Filho, A., Campos, D.A. (Eds.), Tectonic Evolution of South America, vol. 31. International Geological Congress, Rio de Janeiro, pp. 389–449.
Miranda, S.F., Cunha, P.R.C., Caldeira, J.L., Michelon, D., Aragao, F.B., 2016. The Atypical Igneous Sedimentary Petroleum Systems of the Parnaiba Basin: Seismic, Well-Logs and Analogues. AAPG International Conference & Exhibition, Abstracts. https://doi.org/10.1190/ice2016-6471370.
Mizusaki, A.M.P., ThomaZ Filho, A., Milani, E.J., Césero, P., 2002. Mesozoic and cenozoic igneous activity and its tectonic control in the northeastern region of Brazil, South America. J. South Am. Earth Sci., Oxford 15, 183–198. https://doi.org/10.1016/S0895-9811(02)00014-7.
Mohriak, W.U., 2005. Interpretação geológica e geofísica da Bacia do Espírito Santo e da região de Abrolhos: petrografia, datação radiométrica e visual- ização sísmica das rochas vulcânicas. Bol. Geociencias Petrobras 14 (1), 133–142.
Morais Neto, J.M., Pessoa Neto, O.C., Lana, C.C., Zalán, P.V., 2003. Bacias sedimentares brasileiras: bacia do Ceará. Fundação Paleontológica Phoenix 57, 1–6.
Morgan, P., 1983. Constraints on rift thermal processes from heat flow and uplift. Tectonophys. Process. Conti. Rift. 94, 277–298. https://doi.org/10.1016/0040-1951(83)90021-5.
Morrison, J., Burgess, C., Cornford, C., N'zalasse, B., 2000. Hydrocarbon systems of the Abidjan margin, Côte d'Ivoire. In: Offshore West Africa. Fourth Annual Conference, 21–23 March 2000, Abidjan. Pennwell Publishing, Tulsa, OK.
Mougamba, R., 1999. Chronologie et architecture des systemes turbiditiques Cenozoique du prisme sédimentaire de l'Ogooué. (Marge Nord-Gabon). Ph.D. Thesis. Université des Sciences et Technologies de Lille, Lille, pp. 219.
Nemčok, M., Henk, A., Allen, R., Sikora, P.J., Stuart, C., 2012. Continental break-up along strike-slip fault zones: observations from the Equatorial Atlantic. In: In: Mohriak, W.U., Danforth, A., Post, P.J., Brown, D.E., Tari, G.C., Nemčok, M., Sinha, S.T., ST (Eds.), Conjugate Divergent Margins: London, vol. 369. Geological Society, Special Publications, pp. 537–556. https://doi.org/10.1144/SP369.8.
Nzé Abeigne, C.R., 1997. Ph.D. Thesis. Evolution post-rift de la marge continentale Sud-Gabon: contrôles tectonique et climatique sur la sédimentation, vol. 2. Université Montpellier II, pp. 195.
Pellegrini, B.S., Ribeiro, H.J.P.R., 2018. Exploratory plays of Pará-Maranhão and Barreirinhas basins in deep and ultra-deep waters, Brazilian Equatorial Margin. Brazil. J. Geol. v 48 (3), 485–502. https://doi.org/10.1590/2317-4889201820180146.
Pessoa Neto, O.C., 2004. Blocos basculados truncados por discordância angular: lições aprendidas em trapeamento combinado de hidrocarbonetos, Bacia do Ceará, Nordeste do Brasil. Boletim de Geociências Petrobras, Rio de Janeiro 12 (1), 59–71.
Rasmussen, E.S., 1996. Structural evolution and sequence formation offshore South Gabon during the Tertiary. Tectonophysics 266, 509–523. https://doi.org/10.1016/S0040-1951(96)00236-3.
Rohrman, M., 2007. Prospectivity of volcanic basins: trap delineation and acreage de-risking. AAPG Bull. 91 (6), 915–939. https://doi.org/10.1306/12150606017.
Rossetti, D.F., Bezerra, F.H.R., Dominguez, J.M.L., 2013. Late oligocene-miocene transgressions along equatorial and eastern margins of Brazil. Earth Sci. Rev. 123, 87–112. https://doi.org/10.1016/j.earscirev.2013.04.005.
Scarselli, N., Duvel, G., Martin, J., Mc Clay, k., Toothill, S., 2018. Insights into the early evolution of the Côte d'Ivoire Margin (West Africa).Geological Society, London, Special Publications, 476, 16 March 2018. https://doi.org/10.1144/SP476.8.
Schofield, N., Holford, S., Millett, J., Brown, D., Jolley, D., Passey, S., Muirhead, D., Grove, C., Magee, C., Murray, J., Hole, M., Jackson, C., Stevenson, C., 2015. Regional Magma Plumbing and emplacement mechanisms of the Faroe-Shetland Sill Complex: implications for magma transport and petroleum systems within sedimentary basins. Basin Res. 29 (1), 41–63. https://doi.org/10.1111/bre.12164.
Segesman, F.F., 1980. Well-logging method. Geophysics 45 (11), 1667–1684.
Senger, K., Millett, J., Planke, S., Ogata, K., Eide, C.H., Festøy, M., Galland, O., Jerram, D.A., 2017. Effects of igneous intrusions on the petroleum system: a review. First Break: Techn. Article 35 (6), 47–56. https://doi.org/10.3997/1365-2397.2017011.
Séranne, M., Nzé Abeigne, C., 1999. Oligocene to Holocene sediment drifts and bottom currents on the slope of Gabon continental margin (west Africa). Consequences for sedimentation and southeast Atlantic upwelling. Sediment. Geol. 128, 179–199. https://doi.org/10.1016/S0037-0738(99)00069-X.
Séranne, M., Seguret, M., Fauchier, M., 1992. Seismic super-units and post-rift evolution of the continental passive margin of southern Gabon. Bull. Soc. Géol. France 163 (2), 135–146.
Silva Filho, W.F., De Castro, D.L., Corrêa, I.C.S., Freire, G.S.S., 2007. Estruturas rasas na margem equatorial ao largo do nordeste brasileiro (Estado do Ceará): análise de relevo e anomalias gravimétricas residuais. Rev. Bras. Geofís. 25 (1), 65–77. https://doi.org/10.1590/S0102-261X2007000500007.
Silva, S.R.P., Maciel, R.R., Severino, M.C.G., 1999. Cenozoic tectonics of Amazon mouth basin. Geo Mar. Lett. 18, 256–262.
Skogseid, J., Eldholm, O., 1989. Voring plateau continental margin: seismic interpretation, stratigraphy, and vertical movements. In: Eldholm, O., Thiede, J., Taylor, E. (Eds.), Proceedings of the Ocean Drilling Program, Scientific Results. Ocean Drilling Program, College Station, TX, pp. 993–1029.
Skogseid, J., Pedersen, T., Larsen, V.B., 1992. Vøring Basin: subsidence and tectonic evolution. In: In: Larsen, R.M., Brekke, H., Larsen, B.T., Talleras, E. (Eds.), Structural and Tectonic Modelling and its Application to Petroleum Geology, vol. 1. Norwegian Petroleum Society, Special Publications, pp. 55–82. https://doi.org/10.1016/B978-0-444-88607-1.50009-7.
Soares, D.M., Alves, T.M., Terrinha, P., 2012. The breakup sequence and associated lithospheric breakup surface: their significance in the context of rifted continental margins (West Iberia and Newfoundland margins, North Atlantic). Earth Planet Sci. Lett. 355–356, 311–326.
Stagpoole, V., Funnell, R., 2001. Arc magmatism and hydrocarbon generation in the northern Taranaki Basin, New Zealand. Petrol. Geosci. 7 (3), 255–267. https://doi.org/10.1144/petgeo.7.3.255.
Svensen, H., Planke, S., Polozov, A.G., Schmidbauer, N., Corfu, F., Podladchikov, Y.Y.,

Jamtveit, B., 2009. Siberian gas venting and the end-Permian environmental crisis. Earth Planet Sci. Lett. 277 (3–4), 490–500. https://doi.org/10.1016/j.epsl.2008.11.015.

Thomaz Filho, A., Mizusaki, A.M.P., Antonioli, L., 2008. Magmatism and petroleum exploration in the Brazilian Paleozoic basins. Mar. Petrol. Geol. 25 (2), 143–151. https://doi.org/10.1016/j.marpetgeo.2007.07.006.

Tissot, B.P., Welte, D.H., 1984. Petroleum Formation and Occurrence. Springer Verlag, Berlin, pp. 1155.

Trosdtorf Jr., I., Zalán, P.V., Figueiredo, J.J.P., Soares, E.F., 2007. Bacia de Barreirinhas. B. Geoci. Petrobras 15 (2), 331–339.

Vail, P.R., Mitchum, R.M.J.R., Thompson III., S., 1977. Seismic stratigraphy and global changes of sea level, part 3: relative changes of sea level from coastal onlap. In: In: edition, Payton C.E. (Ed.), Seismic Stratigraphy Applications to Hydrocarbon Exploration, vol. 26. AAPG. memoir, pp. 63–97. https://doi.org/10.1306/M26490C5.

Veeken, P.C.H., 2007. Seismic Stratigraphy, Basin Analysis, and Reservoir Characterization. Elsevier Ltd, Oxford.

Wu, C., Gu, L., Zhang, Z., Ren, Z., Chen, Z., Li, W., 2006. Formation mechanisms of hydrocarbon reservoirs associated with volcanic and subvolcanic intrusive rocks: examples in Mesozoic-Cenozoic basins of eastern China. AAPG (Am. Assoc. Pet. Geol.) Bull. 90 (1), 137–147. https://doi.org/10.1306/07130505004.

Zálan, P.V., Warne, J.E., 1985. Tectonics and Sedimentation of the Piauí-Camocim Subbasins, Ceará Basin, Offshore Northeastern Brazil: Série Ciência-Técnica-Petróleo (17). PETROBRAS, Rio de Janeiro, pp. 71.

Zalán, P.V., 2015. Similarities and differences between magma-poor and volcanic passive margins – applications to the Brazilian marginal basins. In: Conference Paper - 14th International Congress of the Brazilian Geophysical Society held in Rio de Janeiro, Brazil, pp. 37–42. https://doi.org/10.1190/sbgf2015-007.

Zalán, P.V., Nelson, E.P., Warme, J., Davis, T.L., 1985. The Piaui Basin: rifting and wrenching in an equatorial Atlantic transform basin. In: In: Biddle, K.T., Christie-Blick, N. (Eds.), Strike-Slip Deformation, Basin Formation, and Sedimentation, Society of Economic Paleontologists and Mineralogists, vol. 37. Special Publication, Tulsa, pp. 177–192. https://doi.org/10.2110/pec.85.37.0177.